

ACCEPTED MANUSCRIPT • OPEN ACCESS

Recent Advances in Near Infrared Upconverting Nanomaterials for Targeted Photodynamic Therapy of Cancer

To cite this article before publication: Carla Arnau del Valle *et al* 2022 *Methods Appl. Fluoresc.* in press <https://doi.org/10.1088/2050-6120/ac6937>

Manuscript version: Accepted Manuscript

Accepted Manuscript is “the version of the article accepted for publication including all changes made as a result of the peer review process, and which may also include the addition to the article by IOP Publishing of a header, an article ID, a cover sheet and/or an ‘Accepted Manuscript’ watermark, but excluding any other editing, typesetting or other changes made by IOP Publishing and/or its licensors”

This Accepted Manuscript is © 2022 The Author(s). Published by IOP Publishing Ltd..

As the Version of Record of this article is going to be / has been published on a gold open access basis under a CC BY 3.0 licence, this Accepted Manuscript is available for reuse under a CC BY 3.0 licence immediately.

Everyone is permitted to use all or part of the original content in this article, provided that they adhere to all the terms of the licence <https://creativecommons.org/licenses/by/3.0>

Although reasonable endeavours have been taken to obtain all necessary permissions from third parties to include their copyrighted content within this article, their full citation and copyright line may not be present in this Accepted Manuscript version. Before using any content from this article, please refer to the Version of Record on IOPscience once published for full citation and copyright details, as permissions may be required. All third party content is fully copyright protected and is not published on a gold open access basis under a CC BY licence, unless that is specifically stated in the figure caption in the Version of Record.

View the [article online](#) for updates and enhancements.

Recent Advances in Near Infrared Upconverting Nanomaterials for Targeted Photodynamic Therapy of Cancer

Carla Arnau del Valle,^a Thomas Hirsch^b and María J. Marín^{*a}

^aSchool of Chemistry, University of East Anglia, Norwich Research Park, Norwich, NR4 7TJ, UK

^bInstitute of Analytical Chemistry, Chemo- and Biosensors, University of Regensburg, 93040 Regensburg, Germany.

*Corresponding author, please direct correspondence to m.marin-altaba@uea.ac.uk.

Abstract

Photodynamic therapy (PDT) is a well-established treatment of cancer that uses the toxic reactive oxygen species, including singlet oxygen ($^1\text{O}_2$), generated by photosensitiser drugs following irradiation of a specific wavelength to destroy the cancerous cells and tumours. Visible light is commonly used as the excitation source in PDT which are not ideal for cancer treatment due to their reduced tissue penetration, and thus inefficiency to treat deep-lying tumours. Additionally, these wavelengths exhibit elevated autofluorescence background from the biological tissues which hinders optical biomedical imaging. An alternative to UV-Vis irradiation is the use of near infrared (NIR) excitation for PDT. This can be achieved using upconverting nanoparticles (UCNPs) functionalised with photosensitiser drugs where UCNPs can be used as an indirect excitation source for the activation of PS drugs yielding to the production of singlet $^1\text{O}_2$ following NIR excitation. The use of nanoparticles for PDT is also beneficial due to their tumour targeting capability, either passively *via* the enhanced permeability and retention (EPR) effect or actively *via* stimuli-responsive targeting and ligand-mediated targeting (*ie.* using recognition units that can bind specific receptors only present or overexpressed on tumour cells). Here, we review recent advances in near infrared upconverting nanomaterials for PDT of cancer with a clear distinction between those reported nanoparticles that could potentially target the tumour due to accumulation *via* the EPR effect (passive targeting) and nanoparticle-based systems that contain targeting agents with the aim of actively target the tumour *via* a molecular recognition process.

Keywords: photodynamic therapy; cancer; upconverting nanoparticles; targeting agents; near infrared

1. Introduction

Photodynamic therapy (PDT) is a minimally invasive treatment that combines the use of light, oxygen and photosensitiser (PS) drugs to generate reactive oxygen species (ROS),^{1,2} being singlet oxygen ($^1\text{O}_2$) the most common cytotoxic oxygen-based molecular species.³ These cytotoxic species are then able to destroy tumours by oxidising biological substrates.³ PS drugs are photoactive molecules able to produce $^1\text{O}_2$ or other ROS after being excited with light of a specific wavelength, most commonly visible or ultraviolet light.² Excited PS can lose their energy *via* fluorescence emission and/or heat;⁴ or following a non-radiative pathway, intersystem crossing, forming a long-lived excited triplet state. From the PS excited triplet state, the energy may decay emitting light or can undergo two different types of reactions yielding radicals and ROS.⁵ Type I reaction is based on an electron or hydrogen transfer and produce radical molecules such as hydroxyl radical (HO^\bullet). In contrast, type II reaction involves an energy transfer from the PS excited triplet state to the ground triplet state of molecular oxygen (O_2) leading the formation of $^1\text{O}_2$.^{4,5}

Apoptosis, necrosis and autophagy are the main cell death pathways that occur by immediate consequence of PDT.^{6,7} Factors such as cell type, light dosage, photosensitiser intracellular localisation and concentration define the mechanism of cell death induced by PDT.⁸ For example, if the PS accumulates in the mitochondria or the endoplasmic reticulum (ER), apoptosis is the main path for cell death.^{7,8} If, by contrast, the PS is targeted either in the plasma membrane or lysosomes, the cells will die *via* necrosis.⁵ An elevated concentration of PS drug or light dose has also been related to a necrotic cell death.⁷ Mitochondrial damage yielding to cytochrome *c* release and formation of the protein apoptosome has been reported due to the acute stress response produced by PDT.⁹

PDT is currently used to treat different types of early-stage cancers including skin,¹⁰ oesophageal,¹¹ mouth¹² and lung¹³ cancer. One of the major advantages of PDT compared to conventional cancer treatments, such as chemotherapy and radiotherapy, is that it is a non-invasive, localised treatment and thus, its side effects are considerably reduced. The combination of PDT with other anticancer therapies has shown synergistic effects.¹⁴⁻¹⁶ For example, PDT has been combined with low doses of X-ray radiation for the treatment of breast cancer cells (MCF-7) in *in vitro* experiments resulting more effective than each treatment alone.¹⁶ The combination of PDT with chemotherapy has been studied in, for example, metastatic melanoma resulting in a higher decrease of metastatic melanoma tumorigenic cells than the decrease observed for the individual treatments.¹⁷

1
2
3 Phthalocyanines, porphyrins, naphthalocyanines, chlorins, bacteriochlorins, texaphyrins, among
4 others, are examples of organic PS drugs commonly reported in the literature for PDT of
5 cancer.^{3,18} Inorganic PS, based on nanoparticles of semiconductor metal oxides (TiO₂ and ZnO)
6 have also been successfully employed for PDT of cancer.^{19,20} The effectiveness of PDT is
7 dependent on the chemical properties, photostability, physiological stability, absorption
8 coefficient and efficiency of ¹O₂ production of the PS drugs.¹ Despite the large number of
9 examples of PS drugs reported in the literature, only a few of these are currently approved by
10 the Food and Drug Administration (FDA) and the European Medicines Agency (EMA) for clinical
11 use,^{21,22} most likely due to the limitations of the reported PS drugs. The majority of them are
12 hydrophobic molecules, thus easily internalised by cells but with restricted transportation
13 through the body.^{1,23} Furthermore, most PS exhibit non-specific biodistribution,²⁴ leading to
14 severe side effects; and their activation to produce ¹O₂ requires of UV-Vis light,²⁵ which are not
15 ideal for cancer treatment due to their reduced tissue penetration, and thus inefficiency to treat
16 deep-lying tumours.²⁶ It is important to mention that PDT is more effectively achieved when the
17 PSs are close enough to the tumour sites due to the short half-time (0.04 μs) and the high
18 reactivity of ¹O₂ after being formed, thus resulting in a ratio of action of *ca.* 0.02 μm.¹⁸
19 Additionally, in the UV-Vis range, there is an elevated autofluorescence background from the
20 biological tissues which hinders optical biomedical imaging. With the aim of overcoming the
21 limitations of UV-Vis excitation, and as it will be detailed later in this review, the use of near
22 infrared (NIR) excitation for PDT has attracted extensive interest in the past decades since it
23 shows minimal light absorption and scattering by biological tissue, thus reducing the
24 photodamage and enabling deeper tissue penetration.^{26,27}

25
26
27
28
29
30
31
32
33
34
35
36
37
38
39
40
41 The use of nanoparticles as delivery systems of PS drugs for PDT has been extensively
42 investigated offering many advantages over molecular PS and overcoming some of the listed
43 drawbacks.²⁸ Incorporation of PS onto nanoparticles can increase the water-solubility of the
44 drugs, elongating their blood circulation time and thus improving their cellular/tumour uptake,
45 pharmacokinetics and biodistribution; and can protect the PS against, for example, enzymatic
46 degradation.²⁹ Additionally, nanoparticles can pass through the leaky blood vessels of tumour
47 sites and accumulate in the malign tissues in a process known as the enhanced permeability and
48 retention (EPR) effect; yielding a passive tumour-targeting.³⁰⁻³² The small size, tailored surface
49 and multi-functionality characteristics of nanoparticles lead furthermore to high drug-loading
50 capacity improving the photostability of the PS and reducing the photobleaching effect normally
51 observed in molecular PS.³² Examples of the most commonly used carrier nanoparticles for PDT
52 include polymeric nanoparticles,³³ liposomes,³⁴ silica nanoparticles³⁵ and metallic nanoparticles
53
54
55
56
57
58
59
60

1
2
3 (such as gold,³⁶⁻³⁹ silver⁴⁰ and iron oxide^{41,42}). For example, Wang *et al.* functionalised gold
4 nanostars with Chlorin e6 (Ce6) and reported higher PDT efficiency both in *in vitro* and *in vivo*
5 when using the nanostars compared to free Ce6.⁴³ The incorporation of PS drugs onto a
6 nanoplatform has been shown to improve the biocompatibility of hydrophobic drugs.^{37,44} For
7 instance, Lee *et al.* developed chitosan nanoparticles loaded with Ce6 for tumour treatment *via*
8 PDT.⁴⁴ Although the ¹O₂ generation was slower for the Ce6 loaded nanoparticles than for the
9 free drug, the Ce6 loaded chitosan nanoparticles were biocompatible showing prolonged blood
10 circulation times and enhanced tumour targeting compared to the free drug.⁴⁴ Nanoparticles
11 have also been reported to increase the PDT effect of some hydrophobic and hydrophilic
12 photosensitiser drugs. For example, Penon *et al.* reported two different functionalised iron oxide
13 nanoparticles containing either hydrophobic or hydrophilic porphyrin derivative ligands.⁴¹ Upon
14 irradiation using a blue light source (400 – 500 nm) both functionalised nanoparticles showed
15 higher levels of ¹O₂ production than the corresponding free porphyrin-based ligands.⁴¹ Alea-
16 Reyes *et al.* studied different types of gold-based vehicles including nanoparticles, nanorods and
17 microparticles, as carriers of porphyrin derivatives for PDT.⁴⁵ The authors reported higher ¹O₂
18 production when using gold nanoparticles and, when used for PDT in HeLa cervical cancer cells,
19 the functionalised gold nanoparticles proved to be more efficient than the corresponding free
20 porphyrin.⁴⁵ An example of polymeric nanoparticles for encapsulation of PS drugs was published
21 by Brandhonneur *et al.* in which poly(D,L-lactide-co-glycolide) (PLGA) nanoparticles were used
22 for the loading of a molybdenum cluster as PS drug leading to encapsulation efficiency higher
23 than 80%.⁴⁶ The loaded PLGA nanoparticles were used for the PDT treatment of ovarian cancer
24 cells (A2780 cell line). Upon irradiation at 365 nm, the molybdenum cluster loaded nanoparticles
25 showed a higher cellular viability decrease (*ca.* 20% higher) compared to the free cluster.⁴⁶ All
26 of these examples prove that nanoparticles are promising carriers of PS drugs for PDT of cancer,
27 overcoming some of the limitations of the free PS drugs and enhancing the efficiency of the
28 treatment. However, one of the persistent problems when using nanoparticles as drug delivery
29 systems is their clearance by the reticuloendothelial system (RES)⁴⁷ which can be overcome by
30 covering them with biocompatible ligands such as proteins, liposomes or polyethylene glycol
31 (PEG); being the incorporation of PEG the most common approach to enhance the water
32 dispersibility of the nanosystems, elongating their circulation time in blood and reducing their
33 RES uptake.⁴⁷ Camerin *et al.* reported PEGylated gold nanoparticles containing a hydrophobic
34 Zn(II)-phthalocyanine derivative as PS for *in vivo* PDT of amelanotic melanoma that resulted in
35 40% of the mice completely recovered following treatment and no tumour regrowth following
36 PDT.³⁶

Another advantage of using nanoparticles for the delivery of PS drugs is that they can be further functionalised with specific targeting molecules to ensure the targeted delivery to the tumour side and thus, the targeted treatment of cancer *via* PDT. Targeting agents such as antibodies, folic acid, transferrin, peptides, aptamers, and carbohydrates, amongst others, are frequently used. For example, Penon *et al.* reported a water-soluble gold nanosystem functionalised with a hydrophobic porphyrin derivative and the antibody anti-erbB2 conjugated to PEG ligands to specifically target the erbB2 receptors expressed in SK-BR-3 breast cancer cells.⁴⁸ High cellular uptake of the antibody-porphyrin-functionalised nanoparticles was observed confirming the antibody-antigen interactions; and PDT induced cell death was achieved following irradiation using a blue light source.⁴⁸

In all the aforementioned examples, the nanoparticles are not directly involved in the photosensitisation process but act as passive carriers of the PS drugs. By contrast, nanoparticles such as quantum dots (QDs)^{49,50} and upconverting nanoparticles (UCNPs)⁵¹⁻⁵³ have been used not only as carriers of PS drugs but as active participants in the PS excitation for PDT of cancer.^{27,49,54,55} Although QDs are excellent candidates in PDT of cancer, this review paper will focus its attention on the use of UCNPs for PDT due to the advantages that indirect NIR excitation of PS drugs through UCNPs present.

2. UCNPs and their role in PDT

UCNPs are nanomaterials capable of converting low energy excitation (NIR) light into high energy emitting photons through an anti-Stokes process which can be separated from other scattered light.^{56,57} UCNPs consist of a crystalline host lattice (hexagonal NaYF₄ being the most efficient to date for green and blue upconversion⁵⁶) containing trivalent lanthanide dopants that act as sensitiser and emitters of energy yielding the upconversion energy transfer process to occur.^{56,58} The sensitiser lanthanide ions (ytterbium ions (Yb³⁺) typically used for 980 nm excitation) can absorb NIR light and transfer two or more photons to the emitting lanthanide ions (the most common are erbium (Er³⁺), holmium (Ho³⁺) and thulium (Tm³⁺)).^{56,59} Cubic or hexagonal NaYF₄ nanoparticles doped with Yb³⁺ and Er³⁺ (NaYF₄ (20%Yb, 2%Er)) result in green or red emissions (522, 541 and 655 nm peaks),⁶⁰ whereas the emission peaks for NaYF₄ (25%Yb³⁺, 0.3%Tm³⁺) nanocrystal are in the blue spectral region (450 nm and 475 nm).⁶⁰ Lanthanide-doped upconverting NaYF₄:Yb³⁺,Er³⁺ nanoparticles are commonly synthesised *via* thermal decomposition of trifluoroacetates in solvent mixtures of oleic acid and octadecene.^{56,61} UCNPs can be also synthesised following other procedures including co-precipitation and hydrothermal

1
2
3 methods.⁶² Importantly, the size, shape, crystal phase and morphology of the nanoparticles can
4 be controlled during the synthesis taking into account parameters such as temperature, dopant
5 concentrations and reaction time resulting in narrow particle size distribution and high
6 reproducibility.^{61,62}
7
8
9

10 The interest in using UCNPs is increasing in fields such as material science, bioimaging and
11 biomedicine due to their intrinsic upconversion luminescent properties.⁶³⁻⁶⁹ They present
12 advantages compared to downconversion systems (quantum dots and fluorescent organic dyes)
13 such as high signal-to-noise ratio, large anti-stokes shifts, non-autofluorescent background,
14 narrow absorption and emission peaks, long lifetimes, high quantum yields and superior
15 photostability, and they have shown to have low toxicity.^{70,71} These lanthanide-doped
16 nanoparticles are chemically stable and in general, less toxic than QDs.⁷¹ In PDT, UCNPs have
17 attracted considerable attention since the first proof-of-concept studies were reported by Zhang
18 *et al.* in 2007.^{72,73} UCNPs overcome the drawback of visible excitation and other limitations of
19 molecular PS including hydrophobicity and non-specificity. In systems consisting of UCNPs
20 functionalised with PS drugs, UCNPs have been used as an indirect excitation source for the
21 activation of PS drugs yielding to the production of singlet $^1\text{O}_2$. The energy transfer between the
22 UCNPs and the PS can take place by radiative (*i.e.* direct absorption of the emitted luminescence
23 photons by the PS drugs) or non-radiative (*i.e.* Förster resonance energy transfer (FRET)
24 mechanism) transitions.⁷⁴
25
26
27
28
29
30
31
32
33
34
35

36 When designing UCNPs functionalised with PS drugs for PDT of cancer, there are several features
37 to be considered (**Figure 1**): (1) the spectral overlap between the light emitted by the UCNPs and
38 the maximum absorption wavelength of the PS; (2) the distance between the inner core of the
39 UCNP and the PS – which is key for an efficient energy transfer; (3) the loading of the PS – which
40 plays an important role in the efficiency of PDT (an excess of PS could inversely affect the PDT
41 effect);⁵⁵ (4) the thickness of the shell, when a core-shell strategy is chosen, since the distance
42 between the PS drug and the luminescence core affects the energy transfer process that
43 activates the PS and thus, the PDT efficiency; (5) the biocompatibility of the nanosystem – which
44 may be increased by introducing ligands such as PEG derivatives; and (6) the targeted PDT
45 strategies – which can be introduced by further functionalisation of PS-loaded UCNPs with
46 targeting agents, thus increasing the specificity and the selectivity of the treatment.
47
48
49
50
51
52
53
54
55
56
57
58
59
60

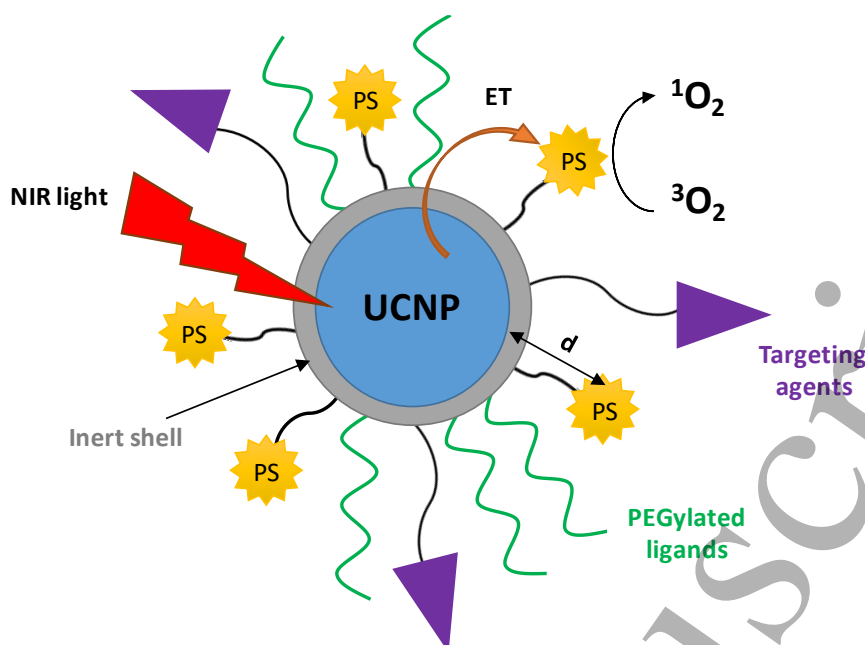


Figure 1. Schematic representation of a core-shell UCNPs functionalised with PS drugs, PEGylated ligands and targeting agents. NIR irradiation of UCNPs generates upconversion luminescence emission which activates the PS drug *via* energy transfer (ET) to produce singlet oxygen ($^1\text{O}_2$) from molecular oxygen ($^3\text{O}_2$).

The surface of UCNPs can be modified with ligand relevant for bioimaging, diagnostics or/and therapeutics *via* ligand exchange, ligand oxidation reaction, host-guest interactions, layer-by-layer self-assembly method, silica encapsulation or coating with amphiphilic polymers.⁷⁵ Loading of PS on the surface of the nanoparticles to obtain an effective electronic excitation energy transfer between the UCNPs and the drug can be achieved following: 1) a non-covalent loading of the PS on the surface of the UCNPs using a silica shell coating (**Figure 2a**) or a physical adsorption which is achieved by using for example amphiphilic polymers (**Figure 2b**);^{55,72,76,77} or 2) a covalent chemical linkage where PS drugs are anchored to the surface of the nanoparticle (**Figure 2c**).^{51,78,79}

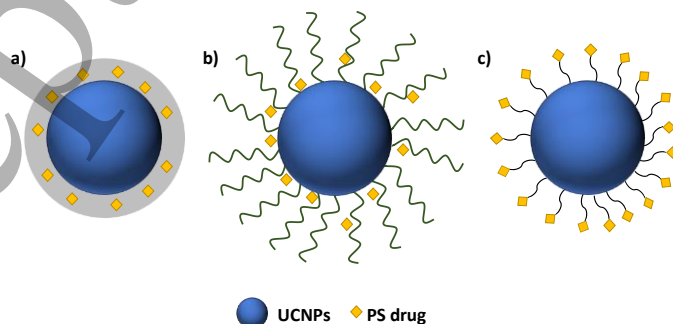


Figure 2. Schematic representation of functionalised UCNPs with PS through **a)** silica encapsulation, **b)** physical adsorption and **c)** covalent chemical bonding strategies.

1
2
3
4
5
6
7
8
9
10
11
12
13
14
15
16
17
18
19
20
21
22
23
24
25
26
27
28
29
30
31
32
33
34
35
36
37
38
39
40
41
42
43
44
45
46
47
48
49
50
51
52
53
54
55
56
57
58
59
60

Ce6 (A_{\max} at *ca.* 400 nm), zinc phthalocyanine (ZnPc) (A_{\max} at *ca.* 660 nm), merocyanine 540 (MC540) (A_{\max} at *ca.* 540 nm), Rose Bengal (RB) (A_{\max} at *ca.* 550 nm) and methylene blue (MB) (A_{\max} at *ca.* 650 nm) are PS drugs commonly used for the functionalisation of UCNPs since their absorption spectrum overlaps with the luminescence emission intensities of commonly used UCNPs. For instance, NaYF₄:Yb,Er nanoparticles exhibit two main luminescence emission wavelengths in the green (522 and 541 nm) and the red (655 nm) regions. This can lead to an effective energy transfer between the NaYF₄:Yb,Er UCNPs and the aforementioned PS drugs and to successful NIR-induced PDT of cancer. Although NaYF₄:Yb,Er are the most commonly used UCNPs for PDT due to their high upconversion efficiency, UCNPs doped with Tm³⁺ have also been reported resulting in luminescence emissions in the blue region (450 and 475 nm) that overlap with PS such as riboflavin, fullerenes, ZnO or TiO₂.

The first example of PS-loaded UCNPs for PDT of cancer was reported by Zhang *et al.* in 2007.⁷² In this work, the PS M-540 was encapsulated onto silica coated NaYF₄:Yb³⁺,Er³⁺ nanoparticles.⁷² Upon irradiation at 974 nm, the UCNPs emitted light at two wavelengths, 537 and 635 nm, with the former effectively overlapping the absorption spectrum of M-540. The M-540-UCNPs were further functionalised with a mouse monoclonal antibody (anti-MUC1/episialin) to specifically target the MUC1 receptors overexpressed in MCF-7/AZ breast cancer cells. Phototoxicity studies performed for MCF-7/AZ cells incubated with the antibody-M-540-UCNPs and irradiated at 974 nm confirmed the effective PDT induced cell death.⁷² Taking this first reported example of targeted agent-PS-UCNPs system as inspiration, a large number of articles can be found in the literature describing the use of PS-UCNPs for the targeted delivery of photosensitiser drugs for PDT of cancer. This review paper provides an in-depth analysis of the most relevant articles reporting the use of UCNPs for targeted-PDT. The review will differentiate between those reported nanoparticles that could potentially target the tumour due to accumulation *via* the EPR effect (passive targeting) and nanoparticle-based systems that contain targeting agents with the aim of actively target the tumour *via* a molecular recognition processes⁸⁰ (active targeting). An schematic representation of the engineering possibilities when designing UCNPs for PDT is given in **Figure 3** and examples of the different approaches will be given in the forthcoming sections of this review paper.

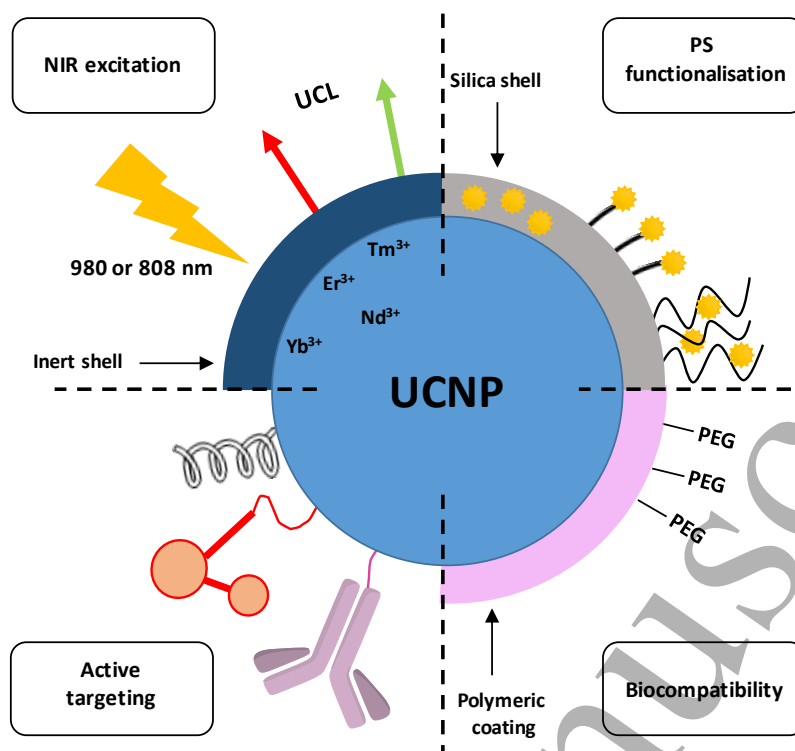


Figure 3. Schematic representation of an UCNP and its engineering possibilities: NIR excitable nanoparticle ($\lambda_{exc} = 980$ or 808 nm) capped with an inert shell, different functionalisation strategies for the incorporation of the PS on the surface of the UCNP, functionalisation with active targeting agents and further coating to enhance the biocompatibility of the nanosystem.

3. Targeted photodynamic therapy using UCNPs

3.1. Passive targeting

The passive targeting of tumour sites using nanoparticles has been extensively exploited for bioimaging and therapeutic applications, including PDT.^{29,54,81,82} The accumulation of the nanoparticles in the solid tumour enhances the specificity of the drug and reduces the side effects on the healthy tissue.^{37,43,44}

A vast number of nanosystems based on PS-UCNPs have been reported to induce cell death *via* NIR triggered PDT. Since the first reported silica shell encapsulation of M-540 PS drug on the surface of the UCNPs by Zhang *et al.*,⁷² a plethora of non-covalent strategies for the incorporation of PS on UCNPs have been described.^{68,76,77,83-88} PS drugs can be encapsulated onto silica shells surrounding the UCNPs using a mesoporous silica layer or a dense silica shell. The mesoporous silica layer provides a larger surface area than the dense silica coating allowing for higher PS loading, thus this has become the preferred approach on the preparation of silica

1
2
3 layered-PS-UCNPs. For example, Zhang and co-workers reported core-shell NaYF₄:Yb,Er@silica
4 nanoparticles functionalised with a mesoporous silica layer loaded with zinc (II) phthalocyanine
5 (ZnPc) (0.1 wt%).⁷⁶ ZnPc was not released from the silica following soaking of the particles in
6 deionised water, phosphate buffer saline or RPMI 1640 cell culture medium for one hour.
7
8 Leaching was however observed when the particles were soaked in ethanol for one hour. The
9 nanoparticles presented an average diameter size of *ca.* 35 nm width and 60 nm length; with a
10 *ca.* 10 nm thickness silica shell and a *ca.* 11 nm mesoporous silica layer. Their red emission band
11 (*ca.* 660 nm) overlapped the absorption peak of the ZnPc (670 nm) allowing the activation of
12 ZnPc to generate ¹O₂ upon irradiation at 980 nm as confirmed measuring the photobleaching of
13 the singlet oxygen probe ABDA (9,10-anthracenediyl-bis(methylene) dimalononic acid) following
14 the endoperoxide formation.⁷⁶ However, lifetime measurements to confirm the FRET process
15 occurring between the UCNPs and the PS drug were not reported. The cellular uptake of the
16 nanoparticles in MB49 bladder cancer cells following 24 h incubation was confirmed using
17 confocal fluorescence microscopy with excitation at 980 nm ($\Delta\lambda_{em} = 525 \pm 50$ nm and 640 ± 90
18 nm). Cell viability studies (3-(4,5-dimethylthiazol-2-yl)-2, 5-diphenyl tetrazoliumbromide, MTT
19 assay) show lower viability for cells incubated with the ZnPc-UCNPs and irradiated at 980 nm
20 (output power of 500 mW, 5 min) than for cells treated with UCNPs without ZnPc and treated
21 under the same conditions. The cellular uptake of the ZnPc-UCNPs was also investigated
22 measuring the intracellular concentration of yttrium over time using inductively coupled plasma-
23 atomic emission spectroscopy (ICP-AES) (maximum Y³⁺ concentration after 6 h of incubation).⁷⁷
24 In this work, the intracellular production of ROS was confirmed in MB49 cells incubated with
25 ZnPc-UCNPs (100 $\mu\text{g mL}^{-1}$) and irradiated at 980 nm (500 mW) using a ROS fluorescent probe (5-
26 (and-6)-carboxy-2'7'-dichlorodihydrofluorescein diacetate) that emits green fluorescence
27 following oxidation in the presence of ROS.⁷⁷ The PDT efficiency of the ZnPc-UCNPs was
28 investigated, using MTT assay, 48 h following NIR irradiation. A drop in cell viability was observed
29 for MB49 cells treated with ZnPc-UCNPs and irradiated for 5 min at 980 nm compared to the
30 corresponding controls (without irradiation and without ZnPc on the UCNPs) – although cell
31 death was observed without irradiation at high dose nanoparticle concentration.⁷⁷ The
32 photodynamic effect of the ZnPc-UCNPs in MB49 cell following 980 nm irradiation was further
33 confirmed by changes in the nuclear morphology – by DAPI staining; intranucleosomal DNA
34 fragmentation – by DNA-ladder agarose gel electrophoresis; cytochrome *c* release – by
35 fluorescence staining of cytochrome *c*; and inhibition of the expression of prostate specific
36 antigen (PSA) – by ELISA.
37
38
39
40
41
42
43
44
45
46
47
48
49
50
51
52
53
54
55
56
57
58
59
60

1
2
3 With the aim of increasing the loading capacity of the PS drug on to the mesoporous silica layer
4 and to avoid the PS leaching, a new strategy was proposed by Han *et al.* in which the authors
5 designed an electrostatic-driven PS loading.^{83,84} NaYF₄:Yb,Er,Nd nanoparticles were coated with
6 a mesoporous silica shell and further functionalised with NH₂ groups resulting in positively
7 charge silica coated UCNPs. Functionalisation of the positively charged UCNPs with the
8 negatively charged Rose Bengal photosensitiser molecules was achieved *via* electronic
9 interactions. In order to prevent the leaching of the PS and to improve the biocompatibility of
10 the nanoparticles, 1-adamantane carboxylic acid molecules were linked to the surface of the
11 UCNPs as guest unit and hydrophilic β -cyclodextrin was used to coat the surface of the RB-UCNPs
12 acting as host molecules.⁸³ The resulting RB-UCNPs (64 \pm 2 nm) were stable to RB leaching in a
13 PBS buffer solution for up to 70 h, as confirmed by UV-Vis measurements.⁸³ Upon irradiation at
14 808 nm, NaYF₄:Yb,Er,Nd nanoparticles exhibited a main emission band centred at 540 nm which
15 overlapped the absorption spectrum of the RB. The effective energy transfer between the
16 UCNPs and the RB was evidenced by the intensity decrease of the upconversion luminescence
17 band at 540 nm in the presence of RB. The ¹O₂ production upon 808 nm irradiation (power
18 density of 4 W·cm⁻²) of RB-UCNPs containing different loadings of RB was monitored using
19 ABMA. The optimal RB content was determined to be 1 wt% since lower concentrations showed
20 less ¹O₂ production and increasing RB concentration led to a reduced ¹O₂ generation possibly
21 due to the self-quenching effect of the RB.⁸³ A comparative study using 808 or 980 nm excitation
22 indicated that the former was superior for penetration and for ¹O₂ generation. The RB-UCNPs
23 were taken up by HeLa cervical cancer cells as confirmed using fluorescence microscopy and
24 recording the intracellular emission of the RB on the UCNPs (whether the RB was excited directly
25 or through the UCNPs was not indicated).⁸³ Using a CCK-8 assay, a significant induced cell death
26 was observed for HeLa cells treated with RB-UCNPs (250 μ g·mL⁻¹) following PDT treatment
27 (808 nm, 1 W·cm⁻², 10 min) compared to the corresponding controls, non-irradiated cells treated
28 with RB-UCNPs. Comparative experiments were performed irradiating HeLa cells with 808 nm
29 and 980 nm light for the same period of time and concluded that the latter resulted in lower cell
30 viability due to an overheating effect.⁸³ This detailed work was preceded by an interesting
31 delivery system reported by the same authors based also on UCNPs nanoparticles coated with
32 a solid silica shell and a mesoporous silica shell containing pore channels.⁸⁴ The photosensitiser
33 methylene blue was embedded in the solid silica shell while RB (as model drug) was loaded in
34 the pores. The novelty of this system lied on the further functionalisation of the particles with a
35 “gatekeeper” to avoid the release of RB from the mesoporous shell. The gatekeeper was a
36 strategically placed ¹O₂-sensitive linker that would only be opened in the presence of ¹O₂
37 releasing the trapped RB. MB was chosen since its absorption spectrum overlaps the emission
38
39
40
41
42
43
44
45
46
47
48
49
50
51
52
53
54
55
56
57
58
59
60

1
2
3 of the UCNPs at 660 nm which undergoes a decrease in intensity, due to the energy transferred
4 to MB, following 980 nm irradiation. The $^1\text{O}_2$ production by the MB-RB-UCNPs and the
5 subsequent release of the RB was confirmed following 980 nm. Cytotoxicity of the nanosystem
6 was observed in A549 lung cancer cells at concentrations higher than $64 \mu\text{g mL}^{-1}$; however, PDT
7 could be performed at lower concentrations ($32 \mu\text{g mL}^{-1}$ UCNPs, 980 nm irradiation for 50 s at
8 $2.0 \text{ W}\cdot\text{cm}^{-2}$). The authors reported also the cell imaging capability of this nanosystem following
9 irradiation at 980 nm.⁸⁴

10
11
12
13
14
15
16 Biocompatible PS drugs like Vitamin B₁₂ (VB₁₂), have also been used with UCNPs for PDT of
17 cancer. Xu *et al.* reported mesoporous-silica-coated NaYF₄:Yb,Er nanoparticles functionalised
18 with VB₁₂.⁸⁵ The NaYF₄:Yb/Er UCNPs emit light at 545 nm ($\lambda_{\text{exc}} = 980 \text{ nm}$) which overlaps the
19 absorption of VB₁₂. MDA-MB-231 breast cancer cells loaded with VB₁₂-UCNPs exhibited a 40%
20 cell viability decrease (MTT assay) following 10 min irradiation at 980 nm.⁸⁵ Control experiments
21 with non-irradiated cells incubated with VB₁₂-UCNPs and irradiated cells incubated with non-
22 functionalised UCNPs confirmed that NIR excitation did not damage the cells and that the
23 designed nanosystem exhibits good biocompatibility under the tested conditions. This work
24 would have benefited from stability studies confirming that the VB₁₂ was still present on the
25 UCNPs when stored overtime.⁸⁵

26
27
28
29
30
31
32
33
34 Although mesoporous silica coated UCNPs functionalised with PS drugs have proven to be
35 efficient for the energy transfer from the UCNPs to the loaded-PS drugs, other approaches to
36 link PS drugs non-covalently to the UCNPs have been reported, including physical adsorption,
37 which results in a more straightforward methodology. For example, the addition of
38 biocompatible ligands or polymers, such as PEG, to the surface of the UCNPs could act as a
39 hydrophobic environment for the incorporation of PS and increase the water-dispersibility and
40 stability of the nanosystem. These biocompatible PS-UCNPs are expected to have increased
41 blood circulation times and consequently higher chance to accumulate in the tumour through
42 the EPR effect. These non-covalent physical adsorption strategies include the entrapping of the
43 PS on an amphiphilic polymeric coating. For instance, Wang *et al.* reported water-soluble
44 PEGylated NaYF₄:Yb,Er nanoparticles functionalised with Ce6 *via* hydrophobic interactions
45 between the PEG chains and the PS with a ca. 8% loading capacity reported.⁸⁶ This was the first
46 article published reporting the potential use of UCNPs for *in vivo* PDT. The Ce6-UCNPs were
47 stable under different physiological conditions (PBS, cell culture medium and foetal bovine
48 serum) and only a 10% Ce6 release was observed in PBS (pH 7.4) after 50 h at room temperature.
49
50
51
52
53
54
55
56
57
58
59
60 The energy transfer from the UCNPs to the Ce6 was confirmed by the quenching of the red

1
2
3 emission band of the naked UCNPs after the loading of the PS. The efficiency of the Ce6-UCNPs
4 for NIR light-activated PDT was investigated both *in vitro* and *in vivo*. Ce6-UCNPs were incubated
5 in 4T1 murine breast cancer cells and a significant reduction in cell viability (MTT assay) was
6 observed following 980 nm excitation (10 min, 0.5 W·cm⁻²) which was not observed when the
7 cells were irradiated following treatment with naked UCNPs or with free Ce6. *In vivo*
8 experiments were performed by intratumoural injection of Ce6-UCNPs in 4T1 murine breast
9 tumour-bearing Balb/c mice and treatment in 980 nm NIR light exposure (0.5 W·cm⁻², 30 min).
10 Two weeks after treatment, the disappearance of the tumour was observed in 7 out of 10 mice
11 and the mice remained alive for up to 60 days (when the mice were put down).⁸⁶ In addition,
12 the tissue penetration ability of the NIR activated PDT in comparison with the direct excitation
13 of the Ce6 on the nanoparticles using 660 nm irradiation was investigated. Although the direct
14 activation of the Ce6 showed higher ¹O₂ generation in solution, a greater tumour reduction was
15 observed following 980 nm irradiation when an 8 mm pork tissue was placed between the laser
16 source and the tumour – simulating deep lying tumours. These results confirmed the higher
17 tissue penetration of NIR light over wavelengths at the visible range and thus the superiority of
18 using PS-UCNPs than the PS drug alone for PDT.⁸⁶ Quantitative biodistribution studies were
19 performed showing that although 1 day following treatment of the tumour with the Ce6-UCNPs,
20 the nanoparticles were found mostly on and close to the skin where they had been injected,
21 their concentration was higher in the liver and spleen 15 days following injection and barely
22 detectable in organs and tissues 60 days following injection. Ce-6 was also used as the PS drug
23 by the same authors to report an improved UCNPs-based drug delivery system for PDT.⁸⁹ In the
24 new approach, the UCNPs were doped with Mn²⁺ to increase the luminescence intensity at
25 660 nm. Ce6 was loaded following a layer-by-layer self-assembly approach yielding 2xCe6-
26 UCNPs which exhibited higher ¹O₂ generation than Ce6-UCNPs. 2xCe6-UCNPs and 980 nm
27 irradiation (0.5 W·cm⁻², 30 min) were used to treat BALB/c mice bearing a 4T1 murine breast
28 cancer tumour inducing, interestingly, a delay in tumour growth when the 2xCe6-UCNPs were
29 injected intratumorally that was not observed when they were administered *via* intravenous
30 injection.⁸⁹

31
32
33 Following a similar non-covalent strategy and using amphiphilic polymer coating, Cui *et al.*
34 reported NaYF₄:Yb,Er nanoparticles, first coated with *N*-succinyl-*N'*-octyl chitosan *via* aqueous
35 phase transfer, doped with ZnPc for *in vivo* PDT.⁶⁸ The loading capacity achieved in this
36 synthesis (10.8%) was higher than those obtained in previous reported example of PS-UCNPs.⁸⁶
37 Using 1,3-diphenylisobenzofuran (DPBF) as the ¹O₂ probe, a 65% decrease in the fluorescence
38 emission of DPBF was observed following 60 min irradiation at 980 nm of the ZnPc-chitosan-

1
2
3 UCNPs, whereas a 3% reduction was obtained for non-irradiated void nanoparticles. $^1\text{O}_2$
4 production of non-irradiated samples of ZnPc-chitosan-UCNPs was not reported by the authors
5 in this paper. ZnPc-chitosan-UCNPs became toxic to human embryonic lung fibroblast (HELFL) and
6 human breast adenocarcinoma (MCF-7) cells when used at high doses ($800 \mu\text{g mL}^{-1}$). A decrease
7 in cell viability was observed in MCF-7 cells loaded with ZnPc-chitosan-UCNPs after irradiation
8 at 980 nm (600 mW, 10 min) compared to the control groups (cells incubated with ZnPc-
9 chitosan-UCNPs and non-irradiated and untreated cells irradiated at 980 nm). Additionally, cell
10 apoptosis in ZnPc-chitosan-UCNPs treated cells exposed to NIR light was confirmed by staining
11 with Annexin V-FITC/PI.⁶⁸ In *in vivo* studies, a slower increase of tumour volume and higher
12 survival rates were observed in S180 sarcoma tumour bearing mice treated with ZnPc-chitosan-
13 UCNPs and irradiated with NIR light than for mice treated only with NIR light, only with ZnPc-
14 chitosan-UCNPs or for non-treated mice. Fluorescence imaging of isolated organs and tumour
15 tissues confirmed that, 14 days after the injection of the ZnPc-chitosan-UNPs, the UCNPs
16 accumulated in the tumour tissue and not in the imaged organs (liver, lung, heart, spleen,
17 intestine and kidney) of the mice.⁶⁸ Meng *et al.* developed another amphiphilic conjugate for
18 the surface modification of UCNPs which permits the adsorption of the PS and enhances the
19 cellular permeability by inhibiting the P-glycoprotein (P-gp) which is overexpressed in cancer
20 cells and obstructs the internalisation of therapeutic agents (**Figure 4**).⁸⁷ Oleate capped
21 NaYF₄:Yb,Er nanoparticles were modified with D- α -tocopherol (vitamin E) polyethylene glycol
22 1000 succinate-succinic acid-mercaptoethylamine (TPGS-SH) following sonication. The resulting
23 TPGS-SH-UCNPs were water-dispersible containing an outer hydrophilic shell and a hydrophobic
24 core due to the vitamin E segments and the oleate chains respectively; and exhibited two
25 emission bands at 540 and 654 nm. The functionalisation of the UCNPs with ZnPc (with
26 maximum absorption wavelength at 664 nm) was successfully achieved through hydrophobic
27 interactions with a loading capacity of 3.05%.⁸⁷ The ZnPc-TPGS-SH-UCNPs exhibited relatively
28 good stability in simulated gastrointestinal media over a period of 6 h with stability in the particle
29 size and reduction of fluorescence intensity of *ca.* 27% after incubation in simulated gastric fluid
30 containing pepsin. The ability of the ZnPc-TPGS-SH-UCNPs to produce $^1\text{O}_2$ was confirmed by the
31 decrease in absorbance of DPBF following excitation at 980 nm. The consumption of DPBF was
32 not observed when particles without ZnPc were irradiated; a control experiment measuring the
33 consumption of DPBF in the presence of non-irradiated ZnPc-TPGS-SH-UCNPs was not reported.
34 *In vitro*, a significant decrease in cell viability was observe in Caco-2 human colon carcinoma cells
35 incubated with ZnPc-TPGS-SH-UCNPs ($100 \mu\text{g mL}^{-1}$) and irradiated at 980 nm (800 mW, 10 min).
36 The control groups, including irradiated unloaded UCNPs and non-irradiated unloaded UCNPs,
37 did not exhibit any cell viability decrease (MTT assay).⁸⁷ The mucosal penetration of the ZnPc-

TPGS-SH-UCNPs, attributed to the thiol-based ligands, was investigated in Sprague-Dawley rats measuring the Y^{3+} concentration and showed the accumulation of the nanoparticles on the enterocytes of duodenum.⁸⁷

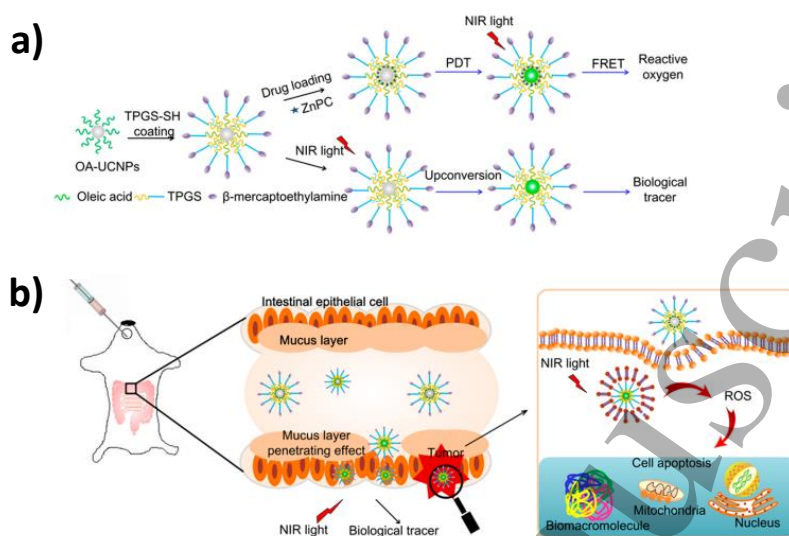


Figure 4. Schematic representation of **a)** ZnPc-TPGS-SH-UCNPs reported by Meng *et al.* and **b)** intestinal distribution, mucosal penetration and subsequent PDT.⁸⁷ Reprinted from Ref. 87 with permission from American Chemical Society.[§]

Although non-covalent strategies for the loading of PS drugs onto the surface of UCNPs present a straightforward approach, the precipitate release of the PS can reduce the efficiency of the treatment and lead to side effects. For instance, Liu *et al.* compared the loading capacity of RB on UCNPs following a non-covalent and a covalent strategy.⁹⁰ The authors covalently attached RB hexanoic acid to amino-functionalised UCNPs *via* amide formation reaction and compared the RB desorption with RB-loaded UCNPs *via* electrostatic interactions. The eluted RB characterised by UV-Vis spectroscopy was 1 order of magnitude higher for the non-covalent RB loading strategy confirming the higher stability of the covalently functionalised RB-UCNPs.⁹⁰ This demonstrates that the use of robust covalent bonds to bind PS – and other cargo – to UCNPs may improve the loading efficiency and stability of the nanosystems ensuring the higher control of the possible leaching and of the overall structure. Additionally, a covalent approach may lead to a better control of the distance between the UCNPs core and the loaded PS, which is key for an efficient energy transfer and thus for the production of 1O_2 in PDT applications.

An effective upconversion energy transfer between the PS and the UCNPs not only relies on the spectral overlap of the PS absorption and the upconverting luminescence emission but the distance between the core and the drug plays also a key role in the effective activation of the PS drug. Longer distances between the PS and the nanocore have been related to a proportional

1
2
3 decrease of the energy transfer resulting in a decrease in $^1\text{O}_2$ generation.^{91,92} Controlling the
4 relative distance between PSs and UCNP probes is challenging when using a non-covalent
5 strategy; however, this parameter can be more easily controlled when designing a covalent
6 chemical bond between the PS and the UCNP. For example, Marín and co-workers covalently
7 bonded RB to UCNP through a L-lysine unit which results in a controlled short distance between
8 the UCNP and the PS.⁵¹ Oleate-capped core-shell $\text{NaYF}_4:\text{Yb,Er,Gd}@ \text{NaYF}_4$ nanoparticles ($17.2 \pm$
9 1.0 nm). were modified *via* a ligand exchange method yielding BF_4^- capped UCNP and the L-
10 lysine ligand was then incorporated replacing the BF_4^- ions. Finally, the lysine-capped UCNP
11 were functionalised with RB *via* classical EDC/NHS chemistry resulting in RB-lysine-UCNP.⁵¹
12 ABMA was used to confirm the ability of the RB-lysine-UCNP to generate $^1\text{O}_2$ upon irradiation
13 at 980 nm. Luminescence lifetime measurements were reported to confirm the efficiency of the
14 FRET from the UCNP to the RB. RB-lysine-UCNP were internalised by SK-BR-3 breast cancer
15 cells as evidenced by the emission of the RB and the UCNP using both, confocal laser scanning
16 microscopy and multi-photon microscopy. Using CellTiter Blue[®] assay, the cell viability of SK-BR-
17 3 cells incubated with the RB-lysine-UCNP and irradiated at 980 nm (200 mW, 6 min) showed a
18 decrease of 67% whereas non-irradiated cells showed a 5% decrease due to the dark toxicity of
19 the RB-lysine-UCNP.⁵¹

20
21
22
23
24
25
26
27
28
29
30
31
32 With the aim of combining the covalent chemical bonding of PS drugs on the surface of UCNP
33 and obtaining water-dispersible and more biocompatible NIR excitable nanosystems for PDT,
34 the incorporation of biologically acceptable ligands in combination with PS drugs has been
35 investigated by several groups. For example, Sun *et al.* covalently functionalised PEGylated
36 UCNP with protoporphyrin IX as PS drug resulting in a water-dispersible nanosystem.⁹³ The
37 protoporphyrin IX structure was modified with jeffamine molecules, to obtain a hydrophilic
38 porphyrin derivative, and a thiolated terminal group was incorporated. Then, PEGylated UCNP
39 were prepared from core-shell $\text{NaGdF}_4:\text{Yb,Er}@ \text{NaGdF}_4$ UCNP (14.2 ± 1.3 nm) and a
40 subsequently “click” reaction between the maleimide group on the UCNP surface and the
41 thiolated porphyrin-jeffamine molecules yielded the porphyrin-UCNP.⁹³ The porphyrin
42 functionalisation of the UCNP was confirmed by UV-Vis spectroscopy (2.0% w/w, porphyrin-
43 jeffamine:UCNP) and the energy transfer from the UCNP to the PS was demonstrated by the
44 quenching of the luminescence emission of the UCNP in the range of 400 – 650 nm which
45 matches the absorption band of the PS. In solution, the porphyrin-UCNP were able to produce
46 $^1\text{O}_2$ following irradiation at 980 nm ($0.5 \text{ W}\cdot\text{cm}^{-2}$) with rates that were slightly higher than those
47 produced by the same concentrations of free porphyrin-jeffamine and by the clinically used
48 HMME (hematoporphyrin mono-methylether) irradiated directly at 635 nm ($0.5 \text{ W}\cdot\text{cm}^{-2}$). The
49
50
51
52
53
54
55
56
57
58
59
60

1
2
3 efficiency of the porphyrin-UCNPs to generate $^1\text{O}_2$ was investigated in an intestinal cancer cell
4 line LS180 using MTT assay. A decrease in cell viability of almost 100% was observed after NIR
5 irradiation (980 nm, $1 \text{ W}\cdot\text{cm}^{-2}$, 10 min) of LS180 cells treated with $1.5 \text{ mg}\cdot\text{mL}^{-1}$ of porphyrin-
6 UCNPs (36 μM porphyrin-jeffamine) whereas the non-irradiated cells incubated with the same
7 concentration of nanoparticles showed a cell viability *ca.* 85%.⁹³

8
9
10
11
12 Natural coating strategies including the incorporation of protein layers (*e.g.* bovine serum
13 albumin (BSA)⁷⁹ and apolipoproteins⁹⁴) or cell membranes⁹⁵ (*e.g.* red blood cells and stem cells)
14 have been also employed for loading PS drugs on the surface of UCNPs. Sabri *et al.* reported the
15 covalent functionalisation of RB on the surface of BSA-UCNPs for PDT of cancer.⁷⁹ First, RB
16 hexanoic acid was covalently linked to the free amine groups of the lysine units present the BSA
17 of BSA-modified $\text{NaGdF}_4\cdot\text{Yb,Er}$ nanoparticles. This work demonstrated the importance that the
18 PS loading concentration has on the effective energy transfer between the UCNPs and the PS.
19 The energy transfer from the UCNPs to the RB was investigated at different RB concentrations,
20 *i.e.* 3, 20 and 30 μM ; the maximum energy transfer (68%) was observed for the particles
21 containing 20 μM RB. Higher concentrations of RB (30 μM) led to a decrease on energy transfer
22 due to the self-quenching between the RB molecules. The NIR activated production of $^1\text{O}_2$ was
23 evidenced using DPBF and monitoring the decrease in absorption intensity at 415 nm following
24 980 nm irradiation. Interestingly, the number of molecules of $^1\text{O}_2$ produced was estimated to be
25 5.9×10^{21} molecules which is above the number of molecules required to produce cell damage
26 (7×10^9).⁹⁶ Confocal microscopy was used to study the cellular uptake of the RB-BSA-UCNPs and
27 to compare it with that of the free RB hexanoic acid and of BSA-UCNPs without RB. Interestingly,
28 RB was localised in the cytoplasm of human lung cancer A549 cells, BSA-UCNPs did not penetrate
29 the cellular membrane and RB-BSA-UCNPs were localised in the cytosol. Therefore, the BSA
30 capping of UCNPs was not involved in the cellular uptake but the conjugated BSA-UCNPs with
31 RB acquire the ability to be internalised by A549 cells. MTT assay was used to study the cell
32 viability of the A549 cells treated with the RB-BSA-UCNPs ($250 \mu\text{g mL}^{-1}$) following 10 min
33 irradiation at 980 nm ($13 \text{ mW}\cdot\text{cm}^{-2}$). Although a 36% cell death was determined for the irradiated
34 cells incubated with RB-BSA-UCNPs, an intrinsic cellular toxicity of 15% was observed without
35 light irradiation. Even though the authors showed an efficient covalent RB loading on the surface
36 of the UCNPs, the ability of those nanosystems to induce cell death *via* PDT could be further
37 improved.

38
39
40
41
42
43
44
45
46
47
48
49
50
51
52
53
54
55
56
57
58
59
60
Stem-cells have been used as biomimetic carriers of UCNPs for PDT resulting in a prolonged
blood circulation time and enhanced tumour passive targeting. The first example of stem-cell
coated UCNPs was reported by Gao *et al.* in 2016 and presented an exhaustive investigation of

1
2
3 the nanoplatform both *in vivo* and *in vitro*.⁹⁷ The authors synthesised NaYF₄:Yb,Er nanoparticles
4 coated with a mesoporous silica layer that exhibited two main luminescence emission bands,
5 green (*ca.* 540 nm) and red (*ca.* 660 nm). Two PS drugs, MC540 (overlaps green emission) and
6 ZnPc (overlaps red emission), were incorporated into the mesoporous silica shell to enhance the
7 PDT effect. Stem-cell-membranes isolated from human and rat bone-marrow-derived
8 mesenchymal stem cells were used to prepare the stem-cell-membrane vesicles *via* physical
9 extrusion method.⁹⁷ Stem-cell-membrane coated UCNPs loaded with MC540 and ZnPc were
10 obtained by an extrusion approach in which the particles were mixed with the previously
11 extruded stem-cell-membranes and passed through 200 nm pore-size polycarbonate membrane
12 11 times. The stem-MC540-ZnPc-mSiO₂-UCNPs had a core size of *ca.* 120 nm and were
13 surrounded by a lipid layer of *ca.* 10 nm in thickness. The size of the stem-MC540-ZnPc-mSiO₂-
14 UCNPs remained stable in solutions containing PBS or foetal bovine serum for up to 2 weeks.
15 The nanocomposites remained stable once taken up by HeLa cells since both the stem-cell-
16 membrane and the UCNPs co-localised in the intracellular environment. The biocompatibility of
17 the designed stem-MC540-ZnPc-mSiO₂-UCNPs was tested by MTT cell viability studies,
18 haemolysis and blood-smear-test; and the three assays confirmed the suitability of the
19 nanoplatform for biological applications. The target-capability of the stem-MC540-ZnPc-mSiO₂-
20 UCNPs was confirmed in HeLa cells using confocal microscopy and by comparison with the
21 reduced internalisation of the particles without stem-cell-membrane by the same cell line. These
22 studies were nicely supported by quantitative studies using flow cytometry where an increase
23 in fluorescence intensity was observed for cells treated with a FITC-labelled stem-MC540-ZnPc-
24 mSiO₂-UCNPs compared to the increase observed for cells treated with FITC-labelled MC540-
25 ZnPc-mSiO₂-UCNPs. To further the applicability of the nanoplatform, *in vivo* tumour-targeting
26 experiments were performed using fluorescence imaging in mice bearing HeLa tumours and
27 following the labelling of the stem-MC540-ZnPc-mSiO₂-UCNPs and MC540-ZnPc-mSiO₂-UCNPs
28 with a NIR excitable dye, Cy7. These studies confirmed the role that the stem-cell-membranes
29 play on the accumulation of the UCNPs in the tumour and on the reduction of the clearance by
30 the RES. The potential of the stem-MC540-ZnPc-mSiO₂-UCNPs as PDT agents was evaluated both
31 *in vitro* and *in vivo*. *In vitro*, HeLa cells were treated with stem-MC540-ZnPc-mSiO₂-UCNPs and
32 controls included cells treated with mSiO₂-UCNPs, MC540-ZnPc-mSiO₂-UCNPs, stem-mSiO₂-
33 UCNPs and PBS. Fluorescence cell staining with a living cell fluorophore (calcein AM) and an
34 apoptosis fluorophore (propidium iodide) and quantitative analysis *via* MTT assay confirmed
35 that only the combination of cells treated with nanoparticles containing the photosensitiser
36 drugs and irradiated at 980 nm (0.35 W·cm⁻², 15 min) yielded to reduce cell viability.
37 Interestingly, stem-MC540-ZnPc-mSiO₂-UCNPs are twice more effective for PDT than MC540-
38
39
40
41
42
43
44
45
46
47
48
49
50
51
52
53
54
55
56
57
58
59
60

1
2
3 ZnPc-mSiO₂-UCNPs without the stem-cell-membranes thus, confirming the targeting ability of
4 the newly developed platform. This complete study concluded with the *in vivo* validation of the
5 system in HeLa cervical tumour-bearing Balb/c mice. The mice were treated under different
6 conditions including PBS, stem-mSiO₂-UCNPs (without PS drugs), MC540-ZnPc-mSiO₂-UCNPs
7 and stem-MC540-ZnPc-mSiO₂-UCNPs all of them following irradiation with 980 nm laser (0.35
8 W·cm⁻¹ for 1 h) or without irradiation. 15 days after the treatment, all the mice were euthanised
9 and the tumour sizes were measured which confirmed that only those mice that had been
10 treated with stem-MC540-ZnPc-mSiO₂-UCNPs following NIR irradiation showed tumour growth
11 inhibition confirming the excellent potential of this novel nanoplatform for *in vivo* PDT.
12
13
14
15
16
17
18

19 Although the majority of the UCNP-based NIR light triggered PDT systems are designed using
20 organic molecules as PS, some semiconductor materials (such as ZnO and TiO₂) have been also
21 employed as inorganic PS. Incorporation of ZnO or TiO₂ shells onto the surface of UCNPs results
22 on an easy PS loading process compared to the surface modifications and PS anchoring
23 approaches when using organic PS drugs. For example, Dou *et al.* reported a core-shell design
24 with UCNPs (NaYF₄:Yb,Tm) as the core and ZnO as the shell (2 – 3 nm width) structure (**Figure**
25 **5**).⁹⁸ The ZnO-UCNPs were further modified with anhydrous sodium citrate to yield water-
26 dispersible UCNPs. The energy transfer between the UCNPs and the ZnO occurs upon irradiation
27 at 980 nm yielding to the disappearance of the luminescence emission band that overlaps the
28 absorbance of ZnO. The ROS production was confirmed by fluorescence spectroscopy, using 3'-
29 (*p*-aminophenyl) fluorescein (ARF) as fluorescent ROS probe.⁹⁸ The ZnO-UCNPs were incubated
30 in two breast cancer cell lines (4T1 and MDA-MB-231 cells) showing good biocompatibility when
31 low nanoparticles concentration was used (10 µg/mL). The PDT effect of the ZnO-UCNPs was
32 evaluated in MDA-MB-231 breast cancer cells by MTT assay using 980 nm irradiation (5 mW) at
33 different times. The results showed a decrease in the cell viability 72 h after treatment (*ca.* 50%)
34 for cells incubated with ZnO-UCNPs and exposed to NIR light for 30 min. UCNPs have also been
35 functionalised with a TiO₂ following different approaches, including the surface coating with a
36 TiO₂ shell⁹⁹ and the conjugation of TiO₂ nanoparticles¹⁰⁰ on the surface of UCNPs. Although the
37 PS-loading of inorganic crystals results in a more straightforward strategy, in most cases, further
38 surface modification is needed to provide the hydrophilicity to the systems.
39
40
41
42
43
44
45
46
47
48
49
50
51
52
53
54
55
56
57
58
59
60

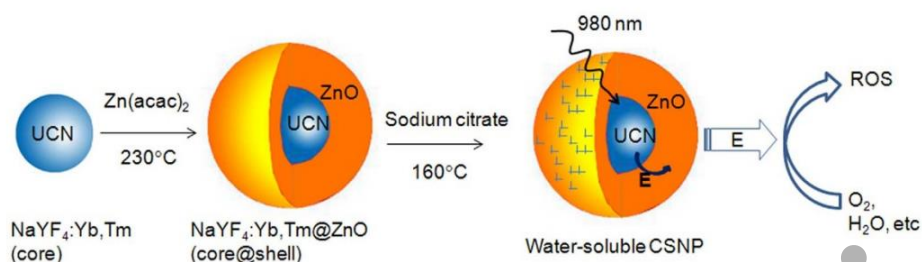


Figure 5. Schematic representation of the ZnO functionalisation of UCNP and the ROS generation upon irradiation at 980 nm.⁹⁸ Reprinted from Ref. 98 with permission from Springer Nature. §§

Other photosensitisers such as transition metal-based complexes (*e.g.* iridium (III) complex¹⁰¹ and ruthenium (II) complex¹⁰²) have been recently combined with UCNP for PDT treatment *in vitro* and *in vivo*. For example, Meijer *et al.* reported the first example of UCNP decorated with a metal-based PS drug for NIR-triggered PDT of cancer.¹⁰² NaYF₄:Yb,Tm nanoparticles (44.2 ± 2.2 nm) exhibited luminescence at 451, 475, 510, 648, 698, 740 and 803 nm when excited at 969 nm, being 451 and 475 nm the desired wavelengths to activate the PS Ru(II) complex. Functionalisation of the UCNP with the Ru(II) complex was performed using a mixture of phospholipids (sodium 1,2-dioleoyl-*sn*-glycero-3-phosphate and 1,2-dioleoyl-*sn*-glycero-3-phosphocholine) and cholesterol in chloroform. A lipid film was formed containing the Ru(II) complex (5 mol%) and the UCNP was hydrated using MES/acetate buffer. A 12% energy transfer between the UCNP and the Ru(II) complex was calculated by combination of steady-state and time-resolved fluorescence spectroscopies.¹⁰² This low energy transfer could be attributed to the long distance between the UCNP core and the PS or due to a low concentration of PS on the surface of the UCNP. Thus, confirming the need of a distance control to enhance the efficiency of the energy transfer which activates the PS to generate the cytotoxic ¹O₂. The Ru(II) complex-UCNP were able to generate ¹O₂ following irradiation at 969 nm (2.0 W, 50 W·cm⁻², 2 h) as indicated by an increase in the absorption intensity of DHFA.¹⁰² Although water-dispersible phospholipid coated Ru(II) complex-UCNP with an excellent overlap between the absorption of Ru(II) complex and the emission of UCNP were successfully synthesised, a low energy transfer was observed between the nanoparticles and the Ru(II) complex limiting the ¹O₂ production and thus the potential of this nanosystems for PDT of cancer.

Recently, a porphyrin-based metal-organic framework has been employed by Shi *et al.* as PS drug for the development of PS-UCNP for PDT of cancer.¹⁰³ The authors stressed the ability of the presented nanoplatform to achieve Type I and Type II PDT *via* NIR excitation and the

1
2
3 reported results addressed this shelling point. A layer of meso-tetra(4- carboxyphenyl)porphine
4 (TCPP)-MOF was grown through a solvothermal process on the surface of NaYF₄:Tm,Yb
5 nanoparticles (*ca.* 29 nm) modified with a polyvinylpyrrolidone (PVP) layer.¹⁰³ The nanoparticles
6 were then coated with a layer of ultra-small TiO₂ nanoparticles which was used as a second PS
7 drug yielding UCNPs-MOF-TiO₂ nanoparticles. Upon excitation at 980 nm the naked UCNPs
8 emitted bands at 291, 344, 360, 450, 475 and 648 nm, which strongly decreased upon addition
9 of the MOF and TiO₂ and thus, confirming the efficient energy transfer between the UCNPs and
10 the other materials. The ability of the UCNPs-MOF-TiO₂ to produce ROS following 980 nm
11 irradiation was determined by monitoring the decrease in the absorbance intensity of DPBF
12 (able to react with several ROS). UCNPs-MOF-TiO₂ were slightly superior in the generation of
13 ROS than UCNPs-MOF. *In vitro* experiments were performed in MCF-7 breast cancer cells. Cells
14 were incubated with UCNPs-MOF-TiO₂ or UCNPs-MOF and further incubated with singlet oxygen
15 sensor green (¹O₂ probe), dihydroethidium (O₂^{•-} probe) and hydroxyphenyl fluorescein (HO[•]
16 probe), irradiated at 980 nm (0.72 W·cm⁻², 5 min) and imaged using the confocal microscope.
17 UCNPs-MOF were able to produce only ¹O₂ while UCNPs-MOF-TiO₂ were able to produce ¹O₂,
18 O₂^{•-} and HO[•], thus probing the ability of the UCNPs-MOF-TiO₂ to be used for Type I and Type II
19 PDT. The efficacy of the UCNPs-MOF-TiO₂ for PDT was further confirmed using MTT assays (and
20 confocal microscopy using propidium iodide staining) reporting a 70% decrease in cell viability
21 only when MCF-7 cells were treated with the nanoparticles and irradiated with NIR light. No
22 decrease was observed in cells treated with the UCNPs-MOF-TiO₂ without irradiation confirming
23 the biocompatibility of the developed nanosystem. Furthermore, MTT assays also reported the
24 superiority of UCNPs-MOF-TiO₂ over UCNPs-MOF to induce cell death *via* PDT following
25 irradiation. The UCNPs-MOF-TiO₂ were also evaluated for *in vivo* PDT using MCF-7 tumor-
26 bearing BALB/c mice. The mice were treated under four different conditions: 1) PBS
27 intravenously injected and no irradiation; 2) PBS intravenously injected and tumour irradiated
28 with a 980 nm NIR laser (0.72 W·cm², light dose 648 J·cm², 15 min); 3) UCNPs-MOF-TiO₂
29 (1 mg/mL, 100 μL) intravenously injected and no irradiation; and 4) UCNPs-MOF-TiO₂ (1 mg/mL,
30 100 μL) intravenously injected and tumour irradiated with a 980 nm NIR laser (0.72 W·cm², light
31 dose 648 J·cm², 15 min). Only those mice treated with the nanoparticles and irradiated with NIR
32 light showed a considerable tumour volume reduction over time with complete disappearance
33 after 90 days and prolonged survival rates for as long as 100 days (the mice in the control groups
34 survived for less than 50 days); thus, confirming the potential of the newly developed platform
35 for PDT of cancer.

3.2 Active targeting

Although a lot of the examples of PDT using UCNPs follow passive targeting strategies taking advantage of the EPR effect,^{51,104} the efficiency of the treatment can be significantly enhanced using active targeting strategies. There are mainly two types of active targeting, stimuli-responsive targeting and ligand-mediated targeting. In the stimuli sensitive approach nanoparticles are tuned to respond to specific changes that occur in the cellular environment of cancer cells but not in healthy cells;⁸⁰ therefore results in a very specific treatment minimising the side effects. This can be achieved by tailoring the surface of the nanoparticles or modifying the PS structure. Another strategy to develop an active targeted PDT is to further functionalise PS-UCNPs with recognition units such as folic acid, antibodies, peptides, carbohydrates, among others, that can bind specific receptors only present or overexpressed on tumour cells.⁸⁰ The use of targeting agents facilitates the uptake of the nanoparticles by cancer cells minimising the undesired side effects.⁸⁰ The following sections in this review paper will be devoted to reporting recent papers describing the development of PS-UCNPs that can be used to target cancer in an active manner, *i.e. via* stimuli-responsive targeting or using ligands that can recognise specific receptors on the cancer cell surface.

3.2.1 Stimuli-responsive targeting

Examples of external stimulus only present on tumour sites include differences on the pH,^{105,106} H₂O₂ concentration¹⁰⁷ or the presence of specific enzymes¹⁰⁸ in the intracellular microenvironments. Delivery platforms are designed bearing this in mind and thus, the PS drugs are just activated when they reach environments that exhibit these specific conditions resulting in an “off-on” strategy. For example, Han and co-workers synthesised UCNPs covalently functionalised with a clinically used prodrug, 5-aminolevulinic acid (ALA), that could be released intracellularly and form the PS protoporphyrin IX only under the acidic environments found in cancer cells.¹⁰⁶ The reported UCNPs consist of cubic phase α -NaYF₄ doped with 80% Yb³⁺ and 20% Er³⁺ as core and CaF₂ as the shell of the nanoparticles (α -NaYF₄:Yb,Er@CaF₂, *ca.* 26 nm). The functionalisation of the UCNPs with ALA was performed through a covalent pH-sensitive hydrazone linked to poly(acrylic acid)-functionalised UCNPs with the aim of the prodrug being released by the lower pH of the endosomes and the subsequent formation of the PS protoporphyrin IX in the mitochondria where it could generate ¹O₂ upon red light excitation.¹⁰⁹ The formation of protoporphyrin IX and the generation of ¹O₂ was confirmed in HeLa cells incubated with ALA-UCNPs (100 μ g mL⁻¹) following irradiation at 980 nm (0.5 W·cm⁻², 10 min)

1
2
3 using a $^1\text{O}_2$ fluorescent probe, 2',7'-dichlorofluorescein diacetate (DCFDA). No $^1\text{O}_2$ production
4 was evidenced in the control group where cells were treated with UCNPs that did not contain
5 ALA (Hyd-UCNPs).¹⁰⁶ MTT assays showed a cell viability decrease of *ca.* 70% after 20 min
6 irradiation at 980 nm that was not observed when the cells were incubated with Hyd-UCNPs or
7 free ALA and irradiated or only irradiated. One of the aims of this research was to increase the
8 deep-tissue treatment by amplifying the red emission of the nanoparticles. To this aim, the
9 authors optimised the content of Yb^{3+} to 80% in solution which was also confirmed in *in vitro*
10 experiments where the PDT effect of ALA-functionalised core-shell cubic nanoparticles α -
11 $\text{NaYF}_4:\text{Yb}(80\%),\text{Er}(2\%)@ \text{CaF}_2$ was compared with that of hexagonal core-shell UCNPs (β -
12 $\text{NaYF}_4:\text{Yb}(20\%),\text{Er}(2%)@ \beta\text{-NaYF}_4$) *via* MTT assay.¹⁰⁶ With the purpose of studying the deeper
13 tissue efficacy of the NIR-triggered PDT, a piece of pork (1.2 cm) was placed between the laser
14 and the cell-containing well. The results showed a decrease in the cell viability of the cells
15 treated with ALA-UCNPs irradiated with NIR light during 40 min through the piece of pork.¹⁰⁶
16 Additionally, *in vivo* experiments were performed in female Balb/c mice treated with ALA-UCNPs
17 comparing the PDT effect following 980 nm irradiation or direct irradiation of the PS. A
18 significant reduction in tumour size was observed for both treatments with no statistically
19 significant differences found between them. However, when a 1.2 cm piece of pork was placed
20 between the tumour side and the laser source, a phototherapeutic effect was observed when
21 980 nm was used as irradiation source, but no tumour size reduction was evidenced when red
22 light excitation was employed. These results further confirm the superiority of using UCNPs in
23 combination with NIR excitation for deep tissue penetration PDT.¹⁰⁶

24
25
26
27
28
29
30
31
32
33
34
35
36
37
38
39 Another example of pH-induced PDT using UCNPs was reported by Feng *et al.*¹⁰⁵ The authors
40 designed RB-UCNPs with a sensitive activation of the $^1\text{O}_2$ generation into tumour acidic
41 environment. The "off-on" strategy was achieved by the incorporation of a pH-sensitive
42 PEGylated polymer and a fluorescence quencher, black hole quencher (BHQ). It is expected that
43 the photoactivity of the nanoplatfrom will be in the "off" state at pH 7.4 in the blood and it will
44 be "turned on" once the nanosystem is internalised in the tumour side and thus reaches
45 environments with lower pH. Core-shell $\text{NaYF}_4:\text{Yb},\text{Er},@ \text{NaYF}_4$ nanoparticles (*ca.* 26 nm) were
46 non-covalently functionalised with RB by mixing the oleate-capped UCNPs with RB hexanoic
47 acid. Next, two PEGylated polymeric micelles were prepared containing RB or BHQ, and were
48 used as polymeric shells for the RB-UCNPs. The $^1\text{O}_2$ generation mediated by pH changes was
49 investigated upon NIR light irradiation using DPBF showing that at pH 5.5 the polymeric shells
50 are released from the particles allowing the recovery of the emission and thus the generation of
51 $^1\text{O}_2$. The cleavage of the polymeric shell was also confirmed measuring the hydrodynamic
52
53
54
55
56
57
58
59
60

1
2
3 diameter of the nanoparticles at both pH values and a decrease in size from 102 nm at pH 7.4 to
4 68 nm at pH 5.5 was observed in agreement with the singlet oxygen production experiments.
5 MCF-7 breast cancer cells were used to evaluate the *in vitro* PDT effect (MTT assay) of three
6 types of nanoparticles: “off-on”-RB-UCNPs which contained PEG polymer ligands with RB and
7 BHQ that were cleaved at acidic pH; “always-off”-RB-UCNPs in which the PEG polymer used
8 contained both RB and BHQ but did not present a pH-cleavable section (negative control); and
9 “always-on”-RB-UCNPs in which the polymer used to build the shell was not modified with the
10 quenchers (positive control). The MCF-7 incubated with “off-on”-RB-UCNPs and irradiated at
11 980 nm ($0.7 \text{ W}\cdot\text{cm}^{-2}$, 15 min) exhibited similar cell viability decrease than those cells incubated
12 with the positive control “always-on”-RB-UCNPs and irradiated. The decrease in cell viability was
13 considerably large compared to the small decrease (*ca.* < 20%) observed when the cells were
14 incubated with “always-off”-RB-UCNPs and irradiated. The paper claims that these results
15 support the theory of activation of the “off-on”-RB-UCNPs when taken up by cancer cells.
16 However, a comparison with the results obtained with healthy cells following the same
17 treatment is essential to support the targeting ability of the particles. The ability of the
18 nanosystem to perform *in vitro* PDT was also confirmed using flow cytometry and staining of
19 apoptotic and necrotic cells which confirms a similar behaviour between “off-on”-RB-UCNPs and
20 “always-on”-RB-UCNPs. The “off-on”-RB-UCNPs were used to image tumour sides in MCF-7
21 tumour bearing mice 4 h after intravenous injection of the nanoparticles. Furthermore, the “off-
22 on”-RB-UCNPs exhibited good biocompatibility and were able to reduce the relative tumour
23 volume following irradiation with 980 nm NIR laser (15 min at 0.6 W cm^{-2}).¹⁰⁵

24
25
26
27
28
29
30
31
32
33
34
35
36
37
38
39 Cancer cells present higher levels of H_2O_2 than normal cells and elevated concentrations of H_2O_2
40 have been associated with malignant cell proliferation.¹¹⁰ Thus H_2O_2 -induced PDT has been
41 investigated as a strategy for the active targeting of cancer cells.¹⁰⁷ For example, Ding *et al.*
42 reported a lanthanide-based nanoplatfrom functionalised with MC540 as PS and MnFe_2O_4 as a
43 Fenton catalyst to generate O_2 from the intracellular H_2O_2 thus potentially enhancing the
44 efficiency of the PDT in cancer cells by increasing tissue penetration (with UCNPs) and reducing
45 hypoxia levels (increasing O_2 concentration at the tumour side).¹⁰⁷ Core-shell $\text{NaYF}_4:\text{Yb,Er}$
46 nanoparticles coated with a mesoporous silica shell *via* silica sol-gel reaction were functionalised
47 with amine groups using 3-aminopropyltriethoxysilane (ATPES). MnFe_2O_4 nanocrystals,
48 prepared following a hydrothermal method and modified with 2-bromo-2-methylpropionic acid
49 (BMPA), were covalently bonded to the amine-functionalised UCNPs *via* nucleophilic
50 substitution reaction. The MnFe_2O_4 -UCNPs were further modified with MC540, which
51 absorption band (540 nm) overlaps one of the luminescence wavelengths of the UCNPs (541
52
53
54
55
56
57
58
59
60

1
2
3 nm). The loading of MC540 on the silica porous was achieved with a 11.52 wt% loading efficiency
4 with no stability studies reported for potential leaching of the PS drug. The MC540-MnFe₂O₄-
5 UCNPs were able to generate O₂ from H₂O₂ in solution. *In vitro* experiments were performed to
6 test the ability of the MC540-MnFe₂O₄-UCNPs to induce the production of ¹O₂ in HepG human
7 liver cancer cells under both, normoxic and hypoxic conditions. A ROS probe, DHFA, and
8 fluorescence microscopy were used to detect the intracellular ¹O₂ formation following
9 treatment of the cells with the MC540-MnFe₂O₄-UCNPs and irradiation at 980 nm (0.5 W·cm⁻²,
10 10 min). A comparative study between MC540-MnFe₂O₄-UCNPs and MC540-UCNPs in HepG cells
11 confirmed the ability of the former to produce ¹O₂ under hypoxic conditions (1% O₂, 5% CO₂ and
12 94% N₂).¹⁰⁷ MTT assays were performed to quantitatively study the *in vitro* PDT effect of MC540-
13 MnFe₂O₄-UCNPs and MC540-UCNPs under normoxic and hypoxic conditions. Both types of
14 nanoparticles (400 µg mL⁻¹) yielded to significant cell mortality when incubated in HepG cells
15 and irradiated at 980 nm (5 min) in normoxic conditions. However, when the cells were
16 incubated under hypoxic atmosphere, a notable difference in cell viability was observed, *ca.* 25%
17 for MC540-MnFe₂O₄-UCNPs and *ca.* 90% for MC540-UCNPs. These results confirmed the higher
18 PDT efficiency of MC540-MnFe₂O₄-UCNPs over MC540-UCNPs in HepG cancer cells due to the
19 ability of MnFe₂O₄ to generate O₂.¹⁰⁷ The incorporation of MnFe₂O₄ onto the UCNPs results not
20 just on a O₂ catalytic generation but also allows the nanoparticles to be magnetically-guided to
21 the tumour sites. The accumulation of the MC540-MnFe₂O₄-UCNPs, injected through the tail,
22 into malignant regions was investigated *in vivo* using BALB/c mice to which H22 mouse
23 hepatoma cells had been subcutaneously injected. Magnetic-guided and non-guided
24 accumulation of the nanoparticles in the tumour was determined by measuring the yttrium
25 concentration by ICP-AES resulting in higher levels of Y³⁺ when a magnetic guidance was
26 applied.¹⁰⁷ The *in vivo* PDT effect of MC540-MnFe₂O₄-UCNPs was then studied in HepG2 tumour
27 bearing nude mice (average tumour volume of 60 mm³) irradiated at 980 nm (10 min). Tumour
28 growth was observed in control groups (treated with PBS or treated with particles without
29 irradiation) in comparison to the impressive tumour inhibition observed for mice treated with
30 MC540-MnFe₂O₄-UCNPs and irradiated which was superior to the observed for mice treated
31 with MC540-UCNPs and irradiated; and thus, may confirm the role that MnFe₂O₄ plays in the
32 generation of O₂ to overcome hypoxia. Additionally, a remarkably *in vivo* PDT improvement was
33 evidenced when administrating MC540-MnFe₂O₄-UCNPs and using magnetic guidance of the
34 nanoparticles to the tumours furthering the great potential of this platform for *in vivo* PDT,
35 imaging and MR.¹⁰⁷ These ambitious examples have confirmed that stimuli-response strategies
36 could be a potential way to reduce the cytotoxicity effects in normal cells. However, the non-
37 specific distribution of the nanoparticles in the body is still an issue and further efforts are
38
39
40
41
42
43
44
45
46
47
48
49
50
51
52
53
54
55
56
57
58
59
60

necessary to deliver the nanoparticles specifically and for them to accumulate in the tumour side. A well-known strategy to achieve this is the incorporation of ligands that can recognise receptors expressed only (or overexpressed) on cancer cells, thus increasing the concentration of PS drugs on the cancer tissue and, therefore, significantly improving the efficiency of the PDT.

3.2.2 Ligands or receptor mediated targeting

The multifunctionalisation capability of UCNPs permits the addition of targeting agents onto the surface of nanoparticles resulting in the specific recognition of the cancerogenic tissue/cells.^{53,63-65,111} Functionalisation of the nanosystems with targeting agents offers advantages over passive targeting such as high specificity and selectivity reducing any adverse effects due to non-targeted toxicities and enhancing the cellular uptake. In general, the active targeted PDT has shown to maximise the accumulation of the PS drugs into malignant tissue and minimise the potential toxicity on normal tissues.⁴⁸

In order to achieve a targeted application, specific targeting agents can be incorporated into the nanoparticle, including monoclonal antibodies^{48,111}, peptides⁶³, aptamers⁵³, carbohydrates^{64,112} and other receptors as folate⁶⁵ and transferrin¹¹³ (Figure 6).

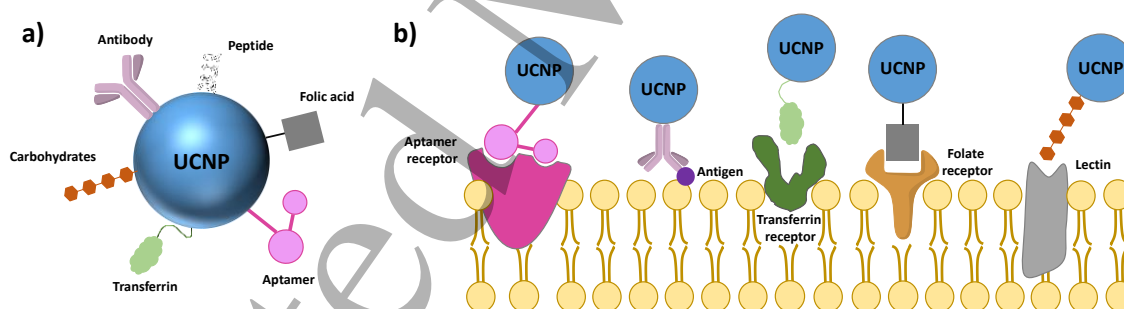


Figure 6. Schematic representation of targeting agents reported in the literature to induce active targeting of cancer cells when UCNPs have been used for PDT of cancer; **a)** UCNP functionalised with the different targeting agents and **b)** specific recognition of the receptors in the cell membrane in each case.

- **Antibodies**

Antibodies are proteins that recognise, highly specifically, other proteins. Some antibodies, such as trastuzumab and cetuximab, have been approved for therapeutics of some types of cancer,¹¹⁴ and a large number of reports describe the modification of drugs and nanoparticles for the targeted delivery to cancer cells. Antibodies were the first targeting agents used to deliver PS-UCNPs specifically to the cancer cells to perform PDT.⁷² In this pioneering work, Zhang *et al.* covalently functionalised the antibody anti-MUC1/episialin onto the surface of the silica capped UCNPs loaded with M-540 as PS to ensure the targeted PDT of breast cancer cells.⁷² Thus, this example was not only the first lanthanide-based nanoparticles designed for PDT but the first active targeted PDT of cancer using UCNPs in combination with a PS drug. Following this initial paper, a large number of papers have reported antibody-PS-UCNPs conjugates for the targeted delivery of the nanoparticles to cancer cells/tissues and thus, with the aim of improving the selectivity of the PDT of cancer.

With the aim of improving the functionalisation of UCNPs with antibodies maintaining the functionality and selectivity of the targeting agent, Liang *et al.* reported a new synthetic strategy in which antibodies were added, in a controlled manner, to the UCNPs through a bifunctional fusion protein.¹¹⁵ Core-shell NaYF₄:Yb,Er@NaGdF₄ nanoparticles were synthesised using a solvothermal decomposition method and coated with a silica layer in the presence of RB using a water-in-oil microemulsion method yielding *ca.* 43 ± 2 nm UCNP@SiO₂(RB). The UCNP@SiO₂(RB) were further modified with a monoclonal antibody following a novel protocol that would allow the control of the orientation of the antibody and thus, minimise the hindrance of the antigen-binding sides during and after the functionalisation process. First, the UCNPs were modified with a bifunctional fusion protein that contained a silica-specific solid-binding peptide – to bind to the silica on the UCNP@SiO₂(RB) – fused to an antibody-binding protein to specifically bind the Fc fragment of the antibody. Once this step was performed, a monoclonal antibody for epithelial cell adhesion molecules (EpCAM; also known as CD326) was added to the nanoparticle conjugate yielding anti-EpCAM-UCNP@SiO₂(RB). Anti-EpCAM functionalisation was confirmed by a negative shift of the zeta-potential values and an increase of the hydrodynamic diameter of the nanoparticles. The energy transfer between the UCNPs and the RB was evidenced by a decrease of the upconversion luminescence emission of the UCNPs at *ca.* 545 nm. The ability of the anti-EpCAM-UCNP@SiO₂(RB) to produce ¹O₂ was tested under 980 nm (1.5 W·cm⁻²) excitation using the DPBF singlet oxygen probe with a 30% of the DPBF consumed after 30 min irradiation. No ¹O₂ production was observed for non-irradiated anti-EpCAM-UCNP@SiO₂(RB) or for irradiated anti-EpCAM-UCNP@SiO₂ confirming the importance of having

1
2
3 the three elements together, UCNP+RB+980 nm excitation, to generate $^1\text{O}_2$. The ability of the
4 anti-EpCAM-UCNP@SiO₂(RB) to specifically target cancer cells was investigated *in vitro* with
5 EpCAM-overexpressing human colon adenocarcinoma HT-29 cells and EpCAM-negative murine
6 microglia BV2 cells. After 1 h incubation, the luminescence emission of the UCNP was observed
7 in the HT-29 but negligible fluorescence was detected in the BV2 cells indicating the specific
8 cellular uptake of the anti-EpCAM-UCNP@SiO₂(RB). To further confirm the targeting ability of
9 the anti-EpCAM-UCNP@SiO₂(RB), UCNP@SiO₂(RB) without antibody were tested in HT-29 cells
10 showing less emission intensity compared to the cells incubated with anti-EpCAM-
11 UCNP@SiO₂(RB). Additionally, a control murine monoclonal antibody CRY104 (non-specific to
12 EpCAM) was conjugated to the UCNP@SiO₂(RB) and incubated in HT-29 cells resulting in an
13 insignificant green emission.¹¹⁵ The intracellular ROS production of the anti-EpCAM-
14 UCNP@SiO₂(RB) upon 980 nm irradiation was confirmed in HT-29 cells using DCFH-DA (that
15 converts to DCFH intracellularly) as $^1\text{O}_2$ probe. A greater increase in the green fluorescence
16 emission intensity due to the formation of DCFH was observed for those cells that had been
17 incubated with anti-EpCAM-UCNP@SiO₂(RB) and exposed to 980 nm irradiation compared to
18 the change observed in the cells treated with anti-EpCAM-UCNP@SiO₂. The PDT effect was also
19 investigated *in vitro* using MTT assay resulting in *ca.* 20% dark cytotoxicity at 200 $\mu\text{g}\cdot\text{mL}^{-1}$ of anti-
20 EpCAM-UCNP@SiO₂(RB). Upon irradiation at 980 nm (1.5 $\text{W}\cdot\text{cm}^{-2}$, 10 min) *ca.* 40% cell viability
21 was obtained indicating the therapeutic effect of the anti-EpCAM-UCNP@SiO₂(RB) in HT-29
22 cells. Furthermore, higher PDT effect was evidenced for the anti-EpCAM-UCNP@SiO₂(RB) than
23 for the corresponding controls, anti-EpCAM-UCNP@SiO₂ and UCNP@SiO₂(RB).¹¹⁵

24
25
26
27
28
29
30
31
32
33
34
35
36
37
38
39 Ramírez-García *et al.* developed ZnPc-NaYF₄:Yb,Er (60% Yb³⁺ and 2% Er³⁺) nanoparticles
40 bioconjugated with trastuzumab for the specific targeted PDT of HER2-positive breast cancer
41 cells.¹¹⁶ First, a ligand exchange reaction to remove the oleic acid from the oleate capped UCNP
42 was performed using cysteamine and then ZnPc molecules were covalently functionalised to the
43 UCNP through carbonamide bond formation between the amine group of the cysteamine (Cys)
44 and the carboxyl group of the ZnPc. The ZnPc-UCNP were then bioconjugated with trastuzumab
45 (TRAS) *via* EDC/NHS chemistry and the concentration of antibody and reaction time were
46 optimised to avoid aggregation or non-specific orientation. The functionalisation of the UCNP
47 was confirmed by measuring the FTIR spectra of the nanoparticles. The TRAS-ZnPc-UCNP
48 showed good colloidal stability and a size of *ca.* 23 nm. The energy transfer between the
49 luminescence at 659 nm and the absorption at 675 nm (ZnPc) upon 975 nm excitation was
50 calculated to be 84.3%.¹¹⁶ ZnPc-UCNP and TRAS-ZnPc-UCNP were able to generate $^1\text{O}_2$ in
51 solution following irradiation at 972 nm (ABMA monitoring) while no obvious production was
52
53
54
55
56
57
58
59
60

1
2
3 observed for the control nanoparticles (Cys-UCNPs). Subsequently, the targeting ability of the
4 TRAS-ZnPC-UCNPs was studied in MCF-7 (HER2-negative) and SK-BR-3 (HER2-positive) breast
5 cancer cells using confocal microscopy with 980 nm excitation. Cys-UCNPs were internalised in
6 both cells lines whereas the ZnPC-UCNPs were not observed in the cells indicating that the
7 uptake of the nanoparticles is diminished when the ZnPc is present on the surface of the UCNPs.
8 Finally, the TRAS-ZnPC-UCNPs were incubated in both cell lines showing only the upconversion
9 luminescence signal on the SK-BR-3 cells. To evaluate The PDT effect of the TRAS-ZnPC-UCNPs,
10 several concentrations of the nanoparticles (0 – 1000 µg/mL) were incubated in both cell lines
11 and the cell viability was measured (XTT assay) after 975 nm (0.71 W·cm⁻², 5 min). Similar
12 cytotoxicity results were obtained for both cell lines when the cells were treated either with Cys-
13 UCNPs or ZnPc-UCNPs. However, higher reductions of the cell viability were observed when SK-
14 BR-3 were incubated with TRAS-ZnPc-UCNPs and irradiated at 975 nm.¹¹⁶ Therefore, the
15 bioconjugation of PS-UCNPs with trastuzumab enable the targeted PDT of cancer cells that
16 overexpress the tyrosine kinase receptor HER2.

17
18 Epithelial growth factor receptors (EGFRs) are commonly overexpressed in lung and breast
19 cancers and in glioblastoma, thus different EGFR-based targeting strategies have been
20 developed using antibodies.¹¹⁷ Zhang and co-workers fabricated UCNPs functionalised with a
21 non-immunoglobulin-derived affinity protein known as Affibody®.¹¹⁸ TiO₂-capped NaYF₄:Yb,Tm
22 nanoparticles were bioconjugated with the anti-EGFR Affibody through a PEG chain. To this aim,
23 dimerised anti-EGFR was first reduced using dithiothreitol (DTT) and then reacted to maleimide-
24 PEG-COOH yielding anti-EGFR-PEG-COOH that was grafted to silane and used for the covalent
25 functionalisation of the TiO₂-UCNPs yielding anti-EGFR-PEG-TiO₂-UCNPs (ca. 50 nm). The
26 antibody functionalisation was confirm using FTIR. The anti-EGFR-PEG-TiO₂-UCNPs show
27 stability after 6 h stored in water and cell culture medium (10% FBS) but not when stored in PBS.
28 The anti-EGFR-PEG-TiO₂-UCNPs were evaluated *in vitro* in a range of cell lines including EGFR-
29 positive cells such as human epidermoid A431 and human lung adenosquamous carcinoma
30 H596, EGFR wild type cells such as lung cancer H460 cells and EGFR-negative cells such as MCF-
31 7 and HepG2 cells. The results presented in the paper indicate the selectivity of the designed
32 nanosystem towards EGFR expressing cells. The work was completed with a detailed *in vivo*
33 evaluation of the anti-EGFR-PEG-TiO₂-UCNPs. The nanoparticles were hemocompatible up to a
34 dose of 50 mg/kg and exhibited 100% survival with no obvious toxic side effects in animals up
35 to 120 days. Furthermore, the *in vivo* PDT effect of the anti-EGFR-PEG-TiO₂-UCNPs was
36 investigated confirming a delay in tumour growth and improved survival rates compared to
37 conventional Ce6 PDT (655 nm).¹¹⁸

- **Folic acid**

Folate receptors (FRs) are overexpressed in many types of cancers including breast, lung, kidney and ovarian. There are 100 – 300 times more FRs in cancer than on healthy cells and they can be divided into three isoforms (FR α , FR β and FR γ) being FR α the most extensively expressed in cancer cells.^{119,120} Folic acid (FA) presents high binding affinity to FRs (dissociation constant (K_D) of 0.1 – 1 nM)¹¹⁹ and, once bound to the FR, FA can be internalised *via* an endocytic transport and accumulated in the cytosol.¹²⁰ Thus, the conjugation of FA with organic molecules and nanoparticles has been used as targeting strategy in cancer diagnosis and therapy. FA (**Figure 7**) has a low molecular weight and high stability; and it contains an acid terminal unit that can be employed to link amino-functionalised molecules or nanoparticles simple and low-cost strategy, *via* an amide formation reaction.¹²⁰ Therefore, FA-mediated active targeting using FA-UCNPs for PDT of cancer cells has been explored providing high sensitivity and specificity towards the detection of several cancer cells reducing the systemic side effects to normal cells.^{90,121-132}

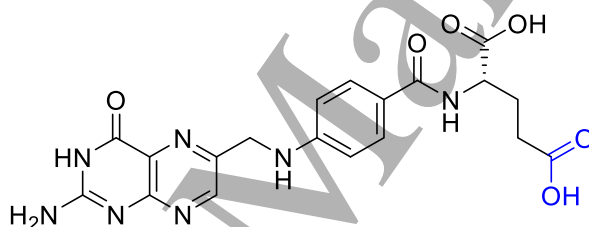


Figure 7. Chemical structure of folic acid; the terminal acid group (**blue**) of the glutamic acid is commonly used to bind other moieties.

The first example of *in vivo* targeted PDT using PS-UCNPs was reported by Idris *et al.* in 2012¹²⁵ where mesoporous silica coated NaYF₄:Yb,Er nanoparticles were functionalised with two PS drugs, MC540 and ZnPc, and FA as targeting agent. The FA-ZnPc-MC540-UCNPs emitted two main upconverting luminescence emissions upon 980 nm irradiation, at 540 and 660 nm, overlapping to the absorption spectrum of MC540 and ZnPC, respectively. Dual-PS-UCNPs exhibited higher ¹O₂ generation than UCNPs singly loaded with either MC540 or ZnPc following 980 nm irradiation (2.5 W·cm⁻², during intervals of 20 min) as observed using ABMA.¹²⁵ The intracellular production of ROS by the dual-PS-UCNPs following 980 nm irradiation (40 min) was confirmed in B16-F0 murine skin cancer cells using DCFDA and confocal microscopy. The control groups, UCNPs functionalised with only one PS and void UCNPs, showed lower ROS production. Only a reduction in cell viability of 55% (MTS assay) was obtained when the B16-F0 cells were

1
2
3 incubated with the dual-PS-UCNPs and irradiated at 980 nm (40 min) whereas a 25% decrease
4 was observed for the void UCNPs showing the cytotoxicity of the UCNPs.¹²⁵ The efficacy of the
5 dual-PS-UCNPs for *in vivo* PDT was investigated injecting the nanoparticles under the skin of
6 C57BL/6 mice bearing B16-F0 melanoma cells and then irradiating at 980 nm (415 mW cm⁻², 2 h)
7 which induced an inhibition of the tumour growth and an enhancement in the population of
8 apoptotic cells as compared to control experiments. A second approach was used in which the
9 dual-PS-UCNPs were intratumorally injected into C57BL/6 mice bearing melanoma tumours and
10 irradiated at 980 nm for 1 h. This treatment slowed the tumour growth during the 11 day period
11 when the mice were monitored. Dual-PS-UCNPs were further functionalised with FA to target
12 the FR overexpressed on B16-F0 cells and PEG to increase the blood circulation time of the
13 UCNPs. Compared to the UCNPs without FA-PEG, the FA-PEG-dual-PS-UCNPs showed a
14 significantly greater reduction in tumour growth when they were intravenously injected in mice
15 bearing B16-F0 melanoma tumours and following NIR irradiation (4 h).¹²⁵ Although better results
16 were obtained after the incorporation of FA and PEG, further optimisation is required since the
17 complete regression of the tumours was not achieved with the reported nanosystem. To this
18 aim, optimisation of the number of encapsulated PS drugs and the porous size of the silica layer
19 can be assessed by determining the maximum energy transfer from the UCNPs to the PSs.

20
21
22
23
24
25
26
27
28
29
30
31
32
33
34
35
36
37
38
39
40
41
42
43
44
45
46
47
48
49
50
51
52
53
54
55
56
57
58
59
60
Incorporation of FA in amphiphilic coated UCNPs has also been investigated for active targeted
PDT of cancer. Thanasekaran *et al.* reported the encapsulation of PS drugs following a
phospholipid coating on the surface of UCNPs.¹²² Compared to PEGylated strategies, lipid
coating results in biocompatible and colloidal stable nanoparticles that are inert to
immunological resistance.¹²² Additionally, the fatty chain of the phospholipid layer enables the
loading of PS drugs through hydrophobic interactions. In this work, oleate-capped NaYF₄:Yb,Er
UCNPs were coated with zwitterionic phospholipids (L- α -phosphatidylcholine (EggPC) and
cholesterol, 1:1 molar ratio) resulting in colloidal stable UCNPs with an average diameter of 40
 \pm 2 nm.¹²² In order to study the PS-loading efficiency of the phospholipid-coated UCNPs, a
screening of several PS drugs, which absorption overlaps the upconversion luminescence bands,
was performed including RB, meso-tetraphenylporphine (TPP), ZnPc, aluminum phthalocyanine
chloride (AlPc), fac-(2,2'-bipyridine)-tricarbonylbromorhenium(I) (Re(bpy)(CO)₃Br),
perinaphthenone (PN) and MB. As expected, the most hydrophobic PS, such as the porphyrin-
based PS, exhibited higher encapsulation efficiency and slower release rates when loaded onto
the phospholipid-coated UCNPs than the less hydrophobic PS.¹²² Determination of ¹O₂
generation by the PS-phospholipid-UCNPs irradiated at 980 nm was performed using p-nitroso-
dimethylaniline (RNO) in the presence of imidazole (RNO + imidazole method). TPP-UCNPs

1
2
3 showed the best performance in the $^1\text{O}_2$ production compared to the rest of PS drugs and were
4 selected for cellular experiments.¹²² The TPP-UCNPs were modified with FA (TPP-UCNP-FA) to
5 assess the targeting ability of the nanosystem. TPP-UCNP-FA nanoparticles were separately
6 incubated in FR-positive KB cells (keratin-forming tumour cell line HeLa) and FR-negative REF52
7 cells (rat embryonic fibroblast) showing higher receptor-mediated cellular uptake in KB cells.
8 PDT studies performed in KB cells and REF52 cells incubated with TPP-UCNP-FA and irradiated
9 at 980 nm (1 h) resulted in greater cell death for FR positive than for FR negative cells (cell
10 viability determined staining the cells with propidium iodide). TPP-UCNP-FA were also
11 investigated for *in vivo* PDT in mice bearing CT-26wt tumours *via* intratumoral injection and
12 following irradiation at 980 nm (1 W cm^{-2} , 30 min). The tumour size was monitored over a period
13 of 10 days and the results showed a very similar tumour growth delay for mice injected with
14 TPP-UCNP-FA and TPP-UCNP and irradiated with NIR light.¹²²

15
16
17
18
19
20
21
22
23
24 Another example of FA-modified amphiphilic coated UCNPs loaded with PS drugs was published
25 by Cui *et al.*¹²⁷ FA-modified amphiphilic *N*-succinyl-*N'*-octyl chitosan (FA-SOC) was first
26 synthesised by amide formation reaction between the carboxyl groups of the FA and the amino
27 groups of the SOC and used to coat previously synthesised oleate-capped $\text{NaYF}_4:\text{Yb,Er}$
28 nanoparticles (*ca.* 50 nm) *via* hydrophobic interactions between the octadecyl groups on the
29 UCNPs and the octyl groups of FA-SOC. ZnPc was trapped into the nanosystem through
30 hydrophobic interactions. The luminescence band at 660 nm (from the excitation for UCNPs at
31 980 nm) was used to activate the ZnPc to generate $^1\text{O}_2$ whereas the second luminescence band
32 (540 nm) was used to image the UCNPs. The highest loading capacity of ZnPc into the amphiphilic
33 chitosan shell was 10%; however, the optimal behaviour was obtained with *ca.* 6% loading. Due
34 to the sensitivity of the chitosan towards acidic pH values (< 6.5), releasing studies of the ZnPc
35 were performed at different pHs (7.4, 6.5 and 5.7) showing less than 20% leaching after 50 h at
36 37 °C in all cases.¹²⁷ The FA-SOC-ZnPc-UCNPs were incubated in human liver cancer Bel-7402
37 cells and imaged using confocal microscopy confirming the intracellular co-localisation of the
38 ZnPc and the UCNPs. Cytotoxicity experiments incubating FA-SOC-ZnPc-UCNPs in human
39 embryo lung HELF and human breast MDA-MB-231 cancer cells showed a negligible decrease in
40 cell viability (using MTT assay) under dark conditions. To investigate the targeting ability of FA-
41 SOC-ZnPc-UCNPs in cells, several cancer cell lines with different levels of FR expression (Bel-
42 7402, MDA-MB231 and A549) were cultured with the same concentration of nanoparticles. The
43 results showed a concomitant relation between the increased uptake of the FA-SOC-ZnPc-
44 UCNPs in cells expressing higher levels of FR. The FA-mediated internalisation was further
45 confirmed with an FR blocking experiment in which before the incubation of the nanoparticles,
46
47
48
49
50
51
52
53
54
55
56
57
58
59
60

FR-positive Bel-7402 and MDA-MB-231 cells were treated with free FA. These results demonstrate the uptake of the FA-SOC-ZnPc-UCNPs in FR-positive cancer cells *via* FR-mediated endocytosis.¹²⁷ After confirming the cellular uptake of the FA-SOC-ZnPc-UCNPs, the intracellular ¹O₂ generation was investigated under 980 nm and 660 nm irradiation for the indirect and direct activation of ZnPc, respectively. To this end, DPBF and DCFDA ROS probes were separately added to Bel-7402 cells incubated with FA-SOC-ZnPc-UCNPs showing in both cases similar results. Higher ROS production was observed when the cells were excited at 660 nm (*ca.* 70%) than when 980 nm laser was used (*ca.* 55%) using the same power density (0.2 W·cm⁻²). When the cells were covered with pork tissue (1 cm), higher ROS generation was determined for cells irradiated at 980 nm (*ca.* 40%) than at 660 nm (*ca.* 15%). *In vivo* studies, performed with FA-SOC-UCNPs (without ZnPc) showed high toxicity of the nanoconstruct when administered at high doses (> 150 mg/kg) and accumulation in the liver, intestines, lungs and kidneys 24 h post injection. The targeting ability of FA-SOC-UCNPs over SOC-UCNPs was also demonstrated *in vivo*. Finally, the PDT treatment was investigated in S180 tumour-bearing mice using 980 nm or 660 nm irradiation conditions. 660 nm irradiation was superior when the tumours were directly exposed to the irradiation; however better results were obtained with 980 nm irradiation when a 1 cm pork tissue was placed over the tumour.¹²⁷

To avoid the leaching of the PS drug from the nanosystem, Zhang and co-workers described UCNPs covalently functionalised with RB and containing FA as targeting agent.⁹⁰ Amine-functionalised NaYF₄:Yb,Er nanoparticles were obtained by ligand exchange using 2-aminoethyl dihydrogenphosphate (AEP) replacing the oleylamine ligands obtained from the synthesis of the UCNPs. RB hexanoic acid was covalently bound to the amine-functionalised UCNPs *via* EDC/NHS chemistry yielding RB-UCNPs (**Figure 8**).⁹⁰ The luminescence spectrum of the UCNPs exhibited a significant decrease of the upconversion luminescence band at 540 nm in the presence of RB on the nanoparticle while the band at 650 nm remained stable; thus, confirming the effective energy transfer from the UCNPs to the RB. The FRET efficiency was estimated to be *ca.* 83%, which is higher than for non-covalent RB encapsulation strategies which reported maximum energy transfer efficiencies of *ca.* 65-68%.^{78,79} The energy transfer was further confirmed by measuring the luminescence decay lifetimes, showing a decrease in the average decay value recorded at 540 nm for the RB-UCNPs.⁹⁰ The production of ¹O₂ by the RB-UCNPs under 980 nm irradiation was examined using DPBF as ¹O₂ probe, showing a 50% decrease in absorption after 16 min irradiation at 980 nm. For the intracellular studies, FA was covalently attached to the surface of the UCNPs through a PEG ligand (NH₂-PEG-COOH) to enhance the targeting efficiency of the RB-UCNPs in cancer cells. FA-RB-UCNPs were incubated at different concentrations in JAR

choriocarcinoma and noncancerous NIH 3T3 fibroblast cells and the targeted-PDT treatment following NIR irradiation was investigated using MTT assay.⁹⁰ The JAR cells showed a significant decrease in the cell viability with an increase of FA-RB-UCNPs concentration while NIH 3T3 cells did not show changes in cell viability. A negligible decrease in cell viability was also observed for the control of non-irradiated cells incubated with.⁹⁰

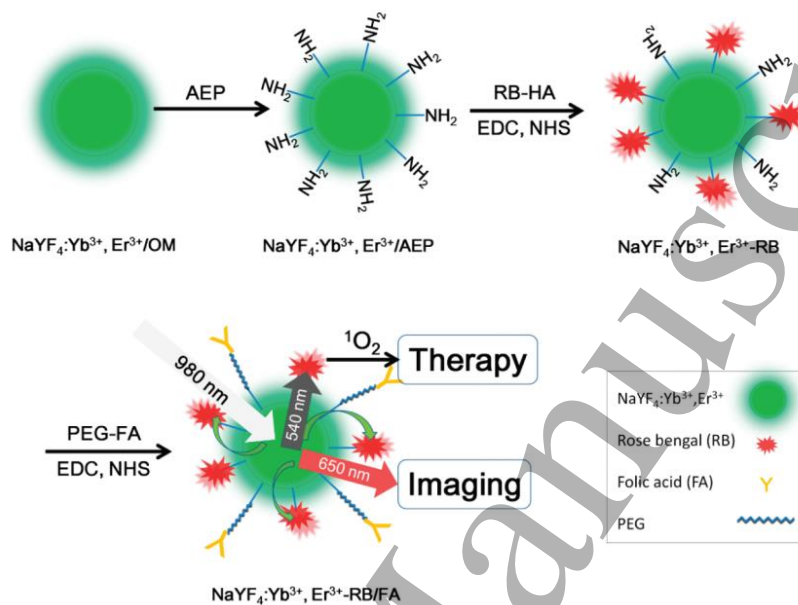


Figure 8. Schematic representation of the preparation of the FA-RB-UCNPs: NaYF₄:Yb,Er UCNPs functionalised with RB, PEG and FA.⁹⁰ Reprinted from Ref. 90 with permission from American Chemical Society. §§§

Another strategy to enhance the energy transfer between the UCNPs and the PS drug is to enhance the upconversion luminescence of the UCNPs. To this aim, different strategies have been developed including the construction of core-shell nanoparticles to avoid any energy losses due to surface defects and/or to increase the doping concentration of the lanthanide ions to enhance the upconversion emission from the UCNPs. Using their previous work as starting point⁹⁰, Zhang and co-workers, designed NaYF₄:Yb,Er UCNPs with 5% additional Yb³⁺ concentration (25% instead of the initial 20%) to increase the upconversion luminescence at 660 nm.¹²⁹ The resulting nanoparticles (*ca.* 30 nm) were coated with poly(allylamine) yielding NH₂-UCNPs. ZnPc (containing carboxyl groups) was covalently attached to the NH₂-UCNPs *via* crosslinking reaction. Additionally, PEG succinimidyl carbonate was incorporated onto the surface of the UCNPs enhancing the dispersibility and stability of the nanoparticles in biological media. Different concentrations of ZnPc were loaded onto the UCNPs and a 6% loading was found to be optimal for the generation of ¹O₂ under 980 nm irradiation (as determined using

1
2
3 DPBF). A comparative study between a covalent and a non-covalent (physical absorption)
4 incorporation of ZnPc onto the UCNPs was performed showing higher $^1\text{O}_2$ production when the
5 PS drug was covalently attached to the nanoparticles.¹²⁹ In order to achieve the specific cancer
6 targeting ability of the nanoparticles, FA was covalently linked to the ZnPc-PEG-UCNPs *via* a
7 cross-linking strategy. Subsequently, the energy transfer between the UCNPs and the ZnPc was
8 determined using steady-state upconverting luminescence spectroscopy and decay kinetics
9 resulting in an 80.9%,¹²⁹ similar to the value obtained for the covalently functionalised RB-UCNPs
10 (83%).⁹⁰ After the confirmation of the outstanding efficiency to generate $^1\text{O}_2$ upon 980 nm
11 irradiation in non-aqueous solution (74% DPBF consumption after 4 min irradiation), FA-ZnPc-
12 PEG-UCNPs were incubated in HeLa cells (FR-positive) and human alveolar adenocarcinoma
13 A549 cells (FR-negative). The upconversion fluorescence images of the incubated cells under 980
14 nm excitation ($0.19 \text{ W}\cdot\text{cm}^{-2}$) showed the efficient cellular uptake *via* FR-mediated endocytosis in
15 FR-positive cells whereas negligible upconversion emission was observed for the FR-negative
16 cells. The targeting capability of the FA ligands was further demonstrated with FR blocking
17 experiments in HeLa cells (previous addition of free FA) showing the absence of fluorescence in
18 the incubated cells upon 980 nm excitation.¹²⁹ The PDT effect of the FA-ZnPc-PEG-UCNPs in HeLa
19 cells upon NIR irradiation was studied using MTT assay and show a significant decrease (70%) of
20 the HeLa cell viability when cells were treated with $200 \mu\text{g}\cdot\text{mL}^{-1}$ of FA-ZnPc-PEG-UCNPs and
21 irradiated at 980 nm ($0.39 \text{ W}\cdot\text{cm}^{-2}$, 10 min). The cell viability results showed considerable dark
22 cytotoxicity of the nanoparticles at concentrations above $200 \mu\text{g}\cdot\text{mL}^{-1}$ whereas a negligible
23 decrease was obtained with lower concentrations. The NIR light induced PDT effects were also
24 investigated *in vivo* using epa1-6 tumour-bearing C57/6J mice. Two weeks following
25 intratumoral injection of the FA-ZnPc-PEG-UCNPs and irradiation at 980 nm (0.39 W cm^{-2} , 15
26 min) a significant reduction in the tumour growth was observed (tumour inhibitory ratio *ca.*
27 80.1%). This effect was not observed for control groups treated with NIR irradiation or FA-ZnPc-
28 PEG-UCNPs only; thus, confirming the PDT effect of irradiated FA-ZnPc-PEG-UCNPs. The
29 behaviour of ZnPc-PEG-UCNPs without FA to fully confirm the targeting ability of the
30 nanoparticles was not investigated in this work.¹²⁹

31
32
33 Wang *et al.* developed UCNPs ($\text{NaYF}_4:\text{Yb}(8\%)/\text{Ho}(1\%)\text{@NaYF}_4:\text{Nd}(20\%)\text{@NaYF}_4$ core-shell-shell)
34 functionalised with RB through an amide coupling reaction using EDC/NHS chemistry in which is
35 the first example reported in the literature with UCNPs excitable at 808 nm for PDT treatment.⁷⁸
36 The $^1\text{O}_2$ production of the RB-UCNPs was investigated in solution using DPBF as $^1\text{O}_2$ probe. A
37 comparative study of PDT performance of RB-UCNPs, depending on the active layer thickness,
38 was performed using 808 nm irradiation showing the larger production of $^1\text{O}_2$ with a shell
39
40
41
42
43
44
45
46
47
48
49
50
51
52
53
54
55
56
57
58
59
60

1
2
3 thickness of 1.6 nm (compared to shells of 0.4, 2.5 and 4.2 nm). HeLa cells were used to confirm
4 the efficiency of the PDT effect *in vitro* following 808 nm excitation and minimisation of the
5 overheating effect when using this irradiation wavelength was confirmed following a
6 comparative study with 980 nm irradiation.⁷⁸
7
8

9
10 Hypericin-loaded NaYF₄:Yb,Er nanoparticles modified with FA were reported by Yang *et al.*¹²⁴
11 The oleate-capped UCNPs were first coated with a silica layer and the photosensitiser hypericin
12 was covalently bound to the silica shell. The absorption band of hypericin at 550 nm overlapped
13 the green luminescence emission of the UCNPs ensuring the effective energy transfer. FA was
14 then conjugated to the surface of the hypericin-UCNPs for the receptor-mediated delivery of the
15 UCNPs.¹²⁴ The production of ¹O₂ by the FA-hypericin-UCNPs under 980 nm irradiation was
16 confirmed using ABMA as a ¹O₂ chemical probe. Two photon laser scanning confocal microscopy
17 was used to study the uptake of the FA-hypericin-UCNPs in FR-overexpressing cancer cells (HeLa
18 cervical cancer cells) and normal cells with lower FR expression (293T embryonic kidney cells),
19 showing higher internalisation of the nanoparticles in HeLa cells. Additionally, the uptake of FA-
20 hypericin-UCNPs and hypericin-UCNPs was compared in HeLa cells resulting in a higher
21 fluorescence emission intensity in the cells when FA-hypericin-UCNPs were incubated,
22 confirming the targeting ability of the FA-hypericin-UCNPs.¹²⁴ The PDT effect of the FA-hypericin-
23 UCNPs was qualitatively investigated using apoptosis assays, staining treated HeLa cells with
24 Annexin V-FITC/PI after irradiation at 980 nm. The fluorescence images of HeLa cells treated
25 with FA-hypericin-UCNPs after NIR irradiation showed apoptotic cells whereas control groups of
26 cells treated with the nanoparticle but without irradiation did not exhibit any indication of the
27 apoptotic process. Flow cytometry was used for the quantitative study of the PDT effect in HeLa
28 cells by FA-hypericin-UCNPs, showing 36% of early and late apoptosis after 15 min irradiation at
29 980 nm of treated HeLa cells.¹²⁴
30
31
32
33
34
35
36
37
38
39
40
41
42
43

44
45 Zhang and co-workers reported core-shell NaYF₄:Yb,Er@NaYF₄:Yb,Tm covalently functionalised
46 with monomalic fullerene (C₆₀MA) as PS drug, PEGylated ligands to enhance the
47 biocompatibility of the nanoparticles and FA as targeting agent.¹²⁸ To achieve the covalent
48 chemical bonding between the ligands and the nanoparticles, UCNPs were first coated with
49 poly(allylamine) providing an amine functionalisation. C₆₀MA was covalently attached to the
50 surface of the amine functionalised UCNPs *via* amide bond formation and a PEGylation process
51 was then performed using PEG-succinimidyl carbonate to increase the water-dispersibility of the
52 C₆₀-UCNPs. The resulting PEG-C₆₀-UCNPs presented a hydrodynamic diameter of 64 nm
53 measured using dynamic light scattering (DLS). The UCNPs exhibited several upconverting
54 luminescence emission bands (450, 475, 540, 650 and 808 nm) following 980 nm irradiation
55
56
57
58
59
60

1
2
3 which overlap (except 808 nm) the broad absorption spectrum of the C₆₀MA. The effective
4 energy transfer between the UCNPs and the C₆₀MA was confirmed using steady state
5 upconversion luminescence measurements and lifetime luminescence decays. Even though the
6 intensities at 450, 475, 540 and 650 nm were all significantly quenched, the maximum energy
7 transfer was calculated to be 79% at 450 nm.¹²⁸ The ¹O₂ production of the PEG-C₆₀-UCNPs was
8 confirmed using fluoresceinyl cypridina luciferin analogue (FCLA) as chemical probe. PEG-C₆₀-
9 UCNPs were further functionalised with FA *via* covalent amine formation between the carboxyl
10 group of the FA and the free amine groups on the surface of the nanoparticles. The resulting FA-
11 PEG-C₆₀-UCNPs were incubated in FR-positive HeLa cells both, using a folate-free and a folate-
12 supplemented medium, and in FR-negative A549 cells and the cellular uptake was monitored
13 recording the emission at 808 nm using confocal microscopy. FA-PEG-C₆₀-UCNPs were taken up
14 by HeLa cells cultured in folate-free medium; however, fewer nanoparticles were internalised in
15 HeLa cells cultured with folate-supplemented medium and in A549 cells. Unfortunately, cell
16 viability studies (MTT assay) showed that very high irradiation power (limits set for human skin
17 exposure to 980 nm light is 0.72 W cm⁻²) and high nanoparticle concentration were needed to
18 induce only a *ca.* 50% viability decrease in HeLa cells incubated with FA-PEG-C₆₀-UCNPs
19 (500 µg·mL⁻¹) and irradiated at 980 nm (1.37 W·cm⁻², 10 min).¹²⁸ The authors claimed that the
20 low PDT efficiency obtained was caused by large distances between the C₆₀ and the core of the
21 UCNPs. To reduce the distance and thus to enhance the energy transfer between the UCNPs and
22 the PS, Zhang and co-workers functionalised core-shell NaYF₄:Yb,Er@NaYF₄:Yb,Tm nanoparticles
23 with C₆₀ following a non-covalent strategy.¹³⁰ A ligand exchange method was used to replace the
24 oleylamine groups on the surface of the UCNPs by C₆₀MA molecules presenting carboxyl groups.
25 Additionally, PEG-block-poly(caprolactone) was incorporated on the C₆₀-UCNPs to enhance the
26 stability of the nanosystems in aqueous solutions. The maximum loading capacity obtained for
27 C₆₀ was found to be 22.5% which was higher than when the covalent strategy was followed
28 (10.5%).¹²⁸ The stability of the PEG-C₆₀-UCNPs was investigated showing a C₆₀ release of 2.5%
29 after 72 h in PBS.¹²⁸ An enhanced in energy transfer between the UCNPs and the PS was obtained
30 by the ligand exchange strategy compared to the covalent assembly, 98.7% and 79% at 450 nm
31 respectively. The ¹O₂ production efficiency was then confirmed using FCLA as chemical probe
32 following irradiation at 980 nm. The results obtained for the ¹O₂ generation of PEG-C₆₀-UCNPs
33 cannot be directly compared to the covalently assembled C₆₀-UCNPs since different
34 concentrations of C₆₀ were loaded in both systems. The PEG-C₆₀-UCNPs were incubated in HeLa
35 cells and the production of ¹O₂ was achieved following 980 nm irradiation (0.39 W·cm⁻², 5 min)
36 as confirmed using DCFDA and fluorescence images.¹³⁰ To achieve targeting, the PEG-C₆₀-UCNPs
37 were further functionalised with FA, directly attached to the PEG units obtaining a FA loading of
38
39
40
41
42
43
44
45
46
47
48
49
50
51
52
53
54
55
56
57
58
59
60

1
2
3 5.1%. The FA-PEG-C₆₀-UCNPs were incubated in HeLa (FR-positive) and A549 (FR-negative) cells
4 and a higher cellular uptake was observed for HeLa cells when monitoring the luminescence at
5 808 nm.¹³⁰ Subsequently, the PDT effect of FA-PEG-C₆₀-UCNPs was studied in HeLa cells (MTT
6 assay) and a 35% viability decrease was observed for cells incubated with FA-PEG-C₆₀-UCNPs
7 (500 µg·mL⁻¹) and irradiated at 980 nm (0.39 W·cm⁻², 10 min). The dark toxicity of the FA-PEG-
8 C₆₀-UCNPs in HeLa cells was negligible at 500 µg·mL⁻¹.¹³⁰ This study concluded that the ligand
9 exchange design of FA-PEG-C₆₀-UCNPs exhibits superior *in vitro* therapeutic effect than the
10 covalently conjugated FA-PEG-C₆₀-UCNPs at lower laser power density. *In vivo* experiments were
11 performed in mice bearing Hepa1-6 tumours (FR-positive) that showed tumour accumulation of
12 tail vein injected FA-PEG-C₆₀-UCNPs 2 h following injection. On the other hand, C₆₀-UCNPs
13 needed 24 h to accumulate in the tumour following injection and as a result of the EPR effect.

14
15
16
17
18
19
20
21
22 Ai *et al.* reported core-shell-shell NaYbF₄:Nd@NaGdF₄:Yb,Er@NaGdF₄ nanoparticles covalently
23 functionalised with Ce6 as photosensitiser and PEGylated modified FA as targeting agent.¹²¹
24 These UCNPs are excitable at 808 nm and emit luminescence at 520 – 560 nm and 650 – 690 nm.
25 The absorption spectrum of Ce6 exhibits a maximum at 660 nm which perfectly overlaps the red
26 luminescence emission peak of the UCNPs. The nanoparticles were first modified with AEP *via*
27 ligand exchange to obtain the amino functionalisation used to covalently attach the Ce6. Finally,
28 the Ce6-UCNPs were capped with FA *via* a dual functionalisation PEGylated unit (NH₂-PEG-
29 COOH).¹²¹ The energy transfer between the UCNPs and the Ce6 was confirmed by steady-state
30 upconversion luminescence measurements showing a 70% efficiency and by luminescence
31 lifetime decays. The production of ¹O₂ by FA-Ce6-UCNPs under 808 nm irradiation increased with
32 increasing Ce6 loading concentrations as observed using DPBF being 10% (w/w) the most
33 effective concentration and thus, the selected for the biological experiments. Experiments of
34 light penetration depth were conducted in solution adding different thicknesses of pork slices
35 between the sample and the laser sources (808 or 976 nm). A decrease in ¹O₂ generation was
36 observed with increasing thickness and deeper tissue penetration was achieved with 808 nm
37 light.¹²¹ *In vitro* experiments using FA-Ce6-UCNPs were performed in KB cells (FR-positive) and
38 A549 cells (FR-negative) and resulted in higher uptake of the nanoparticles by the FR-positive
39 human cancer cells. The intracellular PDT effect of FA-Ce6-UCNPs was investigated and a
40 decrease in cell viability (MTT assay) to 8% was observed for KB cells incubated with the
41 nanoparticles following irradiation at 808 nm. Different concentrations of nanoparticles were
42 tested showing an evident PDT effect after 5 min irradiation when cells were incubated with
43 100 µg mL⁻¹ of FA-Ce6-UCNPs (negligible dark toxicities were observed for this nanoparticle
44 concentration).¹²¹

1
2
3 Zhao *et al.* developed UCNPs with folic acid-polyethylene glycol-poly(aspartic acid-hydrazone)-
4 dihydrolipoic acid (FA-PEAH) polymer chains conjugated to the surface.¹³³ Further
5 functionalisation with pheophorbide a (Pha) as a PS drug *via* an acid-labile hydrazone linker
6 allowed for pH-responsive release of the Pha within the lysosomal compartments of the cells.
7 The emission band of UCNPs at *ca.* 670 nm overlaps with the main absorption band of Pha (broad
8 band at 690 nm) indicating the potential energy transfer between the UCNPs and the PS drug.
9 The successful activation of the Pha upon excitation of the FA-PEAH-UCNPs-Pha at 980 nm was
10 confirmed in solution by detection of the formation of $^1\text{O}_2$ using DPBF as a probe. Intracellular
11 experiments in MCF7 cells proved the improved water dispersibility of the Pha when present on
12 the surface of the UCNPs. Furthermore, FA-PEAH-UCNPs-Pha ($30 \mu\text{g mL}^{-1}$, 980 nm, 0.1 mW cm^{-2} , 5 min)
13 showed higher cytotoxicity than the free Pha confirming the improved PDT treatment
14 when using UCNPs. The FA-PEAH-UCNPs-Pha showed also an enhanced PDT effect compared to
15 the PEAH-UCNPs-Pha confirming the targeting ability of the nanosystem.¹³³ Another example of
16 UCNPs functionalised with FA for targeted PDT was developed by Lim *et al.* in which TCPP was
17 used as PS drug.¹³⁴ Core-shell UCNPs were coated with silica and further functionalised *via*
18 APTED addition with TCPP-NHS, PEG-NHS, and FA/PEG-NHS. The resulting UCNPs@SiO₂-
19 NH₂@FA/PEG/TCPP nanoparticles were tested in HeLa cells showing similar toxicity results for
20 the free TCPP irradiated at 660 nm and for the UCNPs@SiO₂-NH₂@FA/PEG/TCPP irradiated
21 under 808 nm. The cell viability was compared under normoxic and hypoxic conditions showing
22 a significant reduction of the PDT effect in the absence of O₂.¹³⁴

33
34
35
36
37
38
39
40 • **Transferrin**

41
42 The receptor for transferrin (known as TfR1 or CD71) is expressed at low levels in most normal
43 human tissues. However, this receptor is expressed at levels many times higher in malignant
44 cells and thus why it is a popular receptor to target for cancer therapy.¹³⁵

45
46
47 With the aim of targeting these receptors, Liu *et al.* designed transferrin decorated UCNPs for
48 the targeted PDT of cancer cells upon NIR irradiation.¹³⁶ The oleate-capped NaYF₄:Yb,Tm
49 nanoparticles containing 20% Yb and 0.5% Tm were first treated to remove the oleic acid ligands
50 *via* an acid treatment and then functionalised with polyelectrolyte poly[9,9-bis(4'-
51 sulfonatobutyl)fluorine-*alt-co*-(1,4-benzo-(2, 1', 3)-thiadiazole)] sodium salt (PFSBT) as PS and
52 with transferrin (Tf) as targeting agent. The PFSBT-Tf-UCNPs were then further functionalised
53 with a second PS, titanocene (Tc) able to generate free radicals and with high binding affinity
54 toward the iron chelating Tf. Irradiation of the UCNPs at 980 nm resulted in emission peaks at
55
56
57
58
59
60

1
2
3 290, 345, 361, 450, 474 and 800 nm, which, apart from 800 nm, overlapped with the absorption
4 of Tc and the PFSBT. An 87% energy transfer from the UCNP luminescence emission to the PS
5 drugs was estimated at 450 nm and lifetime measurements showed a decrease from 594 to 389
6 μs which also confirmed the energy transfer.¹³⁶ The PFSBT-Tf-Tc-UCNPs were incubated in MCF-
7 7 breast cancer cells to examine the PDT effect of the nanostructures upon 980 nm irradiation
8 (0.6 W·cm⁻²). The photo-cytotoxicity of the PFSBT-Tf-Tc-UCNPs was determined by fluorescence
9 microscopy using calcein acetoxymethylester (Calcein-AM) to stain the live cells and PI to stain
10 the dead cells. The results obtained at different concentrations of PFSBT polymer on the
11 nanoparticles showed an evidence number of dead cells when irradiating at 980 nm UCNP
12 loaded with 10 μg of the PFSBT. Experiments with different concentrations of Tf-Tc on the UCNP
13 were also performed showing an increased cell death when higher amounts were used. *In vivo*
14 PDT experiments using PFSBT-Tf-Tc-UCNPs were performed in a mouse model bearing the H22
15 tumour and showed a significant inhibition of the tumour growth when the animals received the
16 PFSBT-Tf-Tc-UCNPs and irradiation at 980 nm (0.6 W cm⁻², 30 min).¹³⁶

17
18
19
20
21
22
23
24
25
26
27 Transferrin has also been used for the targeted delivery of PS-UCNPs containing also the
28 chemotherapeutic drug doxorubicin (DOX) – dual therapy systems.^{137,138} Zhang *et al.* reported
29 NaYF₄:Yb, Tm:NaYF₄ nanoparticles containing the PS hypocrellin A (HA) incorporated into a
30 mesoporous silica shell that was further functionalised to incorporate DOX *via* silane coupling
31 reaction and a UV cleavable linker (4-(2-carboxy-ethylsulfanylmethyl)-3-nitro-benzoic acid
32 (CNBA) that functions as a gate to permit the controlled release of the drugs.¹³⁷ Finally,
33 transferring was incorporated to the system to achieve targeting delivery of the system. HA-
34 UCNP were able to produce ¹O₂ in solution under irradiation at 980 nm (0.5 W cm⁻²) as
35 monitored using DFBF. The CNBA-DOX-HA-UCNPs showed a photoinduced controlled release of
36 the DOX upon irradiation with NIR light (0.5 W cm⁻²) ascribed to the UV cleavable CNBA linkers.
37 The PDT effect of the CNBA-DOX-HA-UCNPs was evaluated (MTT assay) in HeLa and MCF-7 cells
38 observing a synergistic effect of the dual treatment following irradiation at 980 nm (0.15 W cm⁻²,
39 20 min). Following these studies, Tf was incorporated into the UCNP and the targeting ability
40 of the nanosystem was evaluated in HeLa and MCF-7 cancer cells and 293T normal cells were
41 used as controls. Higher accumulation of Tf-CNBA-DOX-HA-UCNPs was observed compared to
42 CNBA-DOX-HA-UCNPs.¹³⁷ Similar results were obtained by the same authors when Ce6 was used
43 as the PS drug and the enzyme and pH-sensitive linker succinic acid-glycine-phenylalanine-
44 leucine-glycine was used as the gate to release DOX.¹³⁸

- **Peptides**

Peptides have also been used for the targeting of cancer cells since they can enhance the ability to enter the cells (cell penetrating peptides) or they can specifically target tumour epitopes.¹³⁹ In addition, peptides are easy to synthesise, present moderate chemical stability and their small molecular weight allows better tumour penetration. *Trans*-activating transcriptional (TAT) activator is an example of cell penetrating peptides that have been successfully used for intracellular delivery of nanoparticles including micelles, liposomes, quantum dots, UCNPs, polymeric, iron oxide, silica and gold nanoparticles.¹⁴⁰⁻¹⁴² The cancer-associated receptors targeted by peptides include integrins, prostate-specific membrane antigen, transferrin receptor, HER2, aminopeptidase N and CXCR4.¹⁴³ The tripeptide arginine–glycine–aspartic acid (RGD) (**Figure 9**) is commonly used to target cancer cells and preferentially binds to $\alpha_v\beta_3$ integrin receptors which are overexpressed on angiogenic endothelial cells.¹³⁹

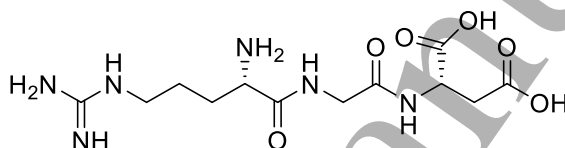


Figure 9. Chemical structure of RGD peptide

Specific peptides with affinity for tumour cells can be combined with PS-nanoparticles to achieve targeted PDT. Peptide-decorated UCNPs have been developed for NIR-activated targeted-PDT of cancer.^{141,142,144-147} For example, Wang *et al.* developed polymer coated UCNPs functionalised with MC540 and RGD peptide to achieve targeted PDT.¹⁴⁴ First, PMAO was grafted with L- α -phosphatidylethanolamine, dioleoyl (DOPE) and RGD peptide. Next, NaYF₄:Yb,Er nanoparticles were coated with the RGD-PMAO-DOPE *via* reverse phase evaporation method resulting in a hydrodynamic diameter of 147 nm. MC540 was trapped into the amphiphilic shell showing a loading efficiency of 9.3%. The ¹O₂ production of MC540-RGD-PMAO-DOPE-UCNPs was confirmed in solution under 980 nm irradiation using ABMA as molecular probe. MC540-RGD-PMAO-DOPE-UCNPs were taken up by MCF-7 breast cancer cells as confirmed by measuring the upconversion luminescence of the UCNPs. The intracellular ROS production was confirmed upon irradiation of cells incubated with MC540-RGD-PMAO-DOPE-UCNPs at 980 nm (ABMA emission measured intracellularly).¹⁴⁴ However, the authors do not report controls of, for example, non-irradiated cells treated with the MC540-RGD-PMAO-DOPE UCNPs to confirm that the observed ROS production was a consequence of the 980 nm irradiation. To investigate the intracellular PDT effect of the nanoparticles, MTS assay of treated MCF-7 breast cancer cells was performed.

1
2
3 A 60% reduction of the cell viability (MTS assay) was obtained after 30 min irradiation of the
4 cells incubated with MC540-RGD-PMAO-DOPE-UCNPs at 980 nm.¹⁴⁴ Although the cell viability
5 decrease obtained for the MC540-RGD-PMAO-DOPE-UCNPs was higher than for the cells treated
6 with MC540-PMAO-DOPE UCNPs without RGD as targeting agent (40%), controls of, for instance,
7 the dark toxicity of the nanoparticles were not performed. Another example, by Hou *et al.*,
8 reports UCNPs decorated with a mesoporous silica shell doped with ZnPc as PS and a cross-
9 linked lipid triple layer formed by PEGylated amphiphilic octadecyl-quaternised polyglutamic
10 acid (OQPGA) which can be further functionalised with cationic RGD peptide.¹⁴⁵ The ZnPc-UCNPs
11 showed an encapsulation efficiency of *ca.* 65%. A 35% ZnPc leached out after 200 min when no
12 crosslinked lipid layer was present and this was reduced to 12.5% in the presence of the lipid
13 layer.¹⁴⁵ The cellular uptake was investigated in HeLa cells substituting the ZnPc by rhodamine
14 to facilitate the fluorescence detection in the microscope. After confirming the co-localisation
15 of the UCNPs and the fluorescence dye by fluorescence microscopy, RGD peptide was
16 incorporated onto the nanoparticles and a slight increase in cellular uptake was observed. The
17 RGD-ZnPc-UCNPs were able to generate ¹O₂ under 980 nm irradiation at higher rates than when
18 free ZnPc was tested (ABMA used as probe). The PDT effect of RGD-ZnPc-UCNPs was evaluated
19 in HeLa cells (MTT assay) showing lower cell viability for cells incubated with RGD-ZnPc-UCNPs
20 and ZnPc-UCNPs and irradiated at 980 nm (1.5 W·cm⁻², 30 min) than when no irradiation was
21 applied. High irradiation power was needed to achieve these results.¹⁴⁵ Although the authors
22 proved the efficiency of the cross-linked lipid layer on the UCNPs reducing the leaching of the
23 PS drug and enhancing the stability of the nanoparticles, additional experiments are required to
24 demonstrate the targeting activity of the nanoparticles decorated with RGD peptide. For
25 instance, tests of the PDT effect *in vivo* will validate the selectivity of the UCNPs to reduce the
26 tumour size *via* PDT.

27
28
29
30
31
32
33
34
35
36
37
38
39
40
41
42
43
44 The aspartyl residue of the linear RGD can suffer a chemical degradation and thus cause the lack
45 of biological activity. The stability against enzymatic degradation of the RGD peptides can be
46 enhanced by using cyclic RGD derivatives.¹⁴⁸ An example of cyclic RGD peptide for targeted PDT
47 using UCNPs was published by Zhou *et al.* and involved NaYF₄:Yb,Er nanoparticles modified with
48 *o*-carboxymethylated chitosan and further functionalised with cyclic Arg-Gly-Asp-(D)-Tyr-Lys
49 (c(RGDyK)) and Ppa as PS drug through the carboxyl groups and the amine groups of the *o*-
50 carboxymethylated chitosan, respectively.¹⁴⁶ Ppa was loaded at 2.8 mg Ppa/mg UCNPs and the
51 RGD-Ppa-UCNPs exhibited high stability at different pH (5, 7.4 and 8) for 24 h. The RGD-Ppa-
52 UCNPs were able to produce higher amount of ¹O₂ when irradiated at 635 nm (20 mW cm⁻²)
53 compared to free Ppa (FCLA used as probe).¹⁴⁶ *In vitro* experiments were then performed to
54
55
56
57
58
59
60

1
2
3 study the $\alpha_v\beta_3$ integrin targeting capacity of the RGD-Ppa-UCNPs. Integrin positive cells (U87-
4 MG brain cancer cells) and integrin negative cells (MCF-7 breast cancer cells) were incubated
5 with RGD-Ppa-UCNPs and the intracellular production of ROS was measured using DCFA upon
6 irradiation at 980 nm ($0.5 \text{ W}\cdot\text{cm}^{-2}$). Higher production of $^1\text{O}_2$ was observed for the integrin
7 positive cell line. The $\alpha_v\beta_3$ integrin-mediated endocytosis of the nanoparticles was confirmed
8 with control experiments where the U87-MG cells were pre-treated with an excess of free
9 c(RGDyK) which showed very low uptake. The PDT effect of RGD-Ppa-UCNPs was also
10 investigated using CCK8 cell viability assay with U87-MG and MCF-7 cells resulting in a significant
11 difference between both cells lines, 60% and 15% reduction, respectively, following irradiation
12 at 980 nm ($0.5 \text{ W}\cdot\text{cm}^{-2}$).¹⁴⁶ The reported nanosystem showed higher $^1\text{O}_2$ generation than the free
13 PS drug, elevated stability and specific binding to the integrin $\alpha_v\beta_3$ -positive tumour cells. *In vivo*
14 experiments would be relevant to confirm the benefit of NIR activated PDT for deep-seated
15 tumours and to further confirm the targeting activity of the RGD-Ppa-UCNPs.

16
17
18
19
20
21
22
23
24
25
26 Another targeting moiety based on peptides is the TAT protein which is a cell penetrating
27 peptide that can be used as intracellular drug delivery vector. For example, Zhang *et al.* reported
28 core-shell-shell NaYbF₄:Nd@NaGdF₄:Yb,Er@NaGdF₄ nanoparticles functionalised with Ppa as PS
29 drug, PEG and TAT peptide.¹⁴² The oleate-capped UCNPs were first modified with PMAO-PEG-
30 NH₂ allowing the covalent functionalisation of the TAT. Then, Ppa was loaded onto the surface
31 of the PMAO-PEG-TAT-UCNPs *via* hydrophobic interactions resulting in a loading capacity of 0.6
32 mg Ppa/mg UCNPs. The $^1\text{O}_2$ generation upon 808 nm irradiation of the Ppa-UCNPs at different
33 loading concentrations (0.025, 0.05, 0.1 and 0.2 ratios) was confirmed using DPBF as chemical
34 probe with the best results obtained when using a loading amount of Ppa of 0.05 mg Ppa/mg
35 UCNPs. The Ppa-UCNPs were stable in a PBS buffer solution (pH 7.4) for a minimum of 4 h.¹⁴²
36 Subsequently, TAT modified UCNPs exhibited a higher cellular uptake in HeLa cells than UCNPs
37 without TAT – as determined by quantification of Gd concentrations using ICP-OES. Intracellular
38 generation of ROS upon irradiation at 808 nm was observed in HeLa cells incubated with the
39 modified UCNPs using DCFDA as fluorescent molecular probe. These results agree with the
40 significant decrease in the cell viability following 808 nm irradiation ($6 \text{ W}\cdot\text{cm}^{-2}$, 5 min).¹⁴² Co-
41 localisation studies were performed showing the majority of the Ppa accumulated in the same
42 cytoplasmic region of HeLa cells than the UCNPs verifying the stability of the Ppa-UCNPs after
43 their internalisation into the cells. Ppa was localised in the mitochondria as confirmed by co-
44 localisation studies using MitoTracker green. Additionally, JC-1 assay was used to monitor the
45 damage in the mitochondria upon 808 nm irradiation of cells incubated with Ppa-UCNPs,
46 confirming the potential of the nanosystem for mitochondria-targeted PDT.¹⁴² However,
47
48
49
50
51
52
53
54
55
56
57
58
59
60

1
2
3 although the authors demonstrate the phototherapeutic efficiency of the Ppa-UCNPs and the
4 enhanced cellular uptake when TAT peptide was present, it is important to note that the power
5 of laser used in this work is extremely high and not applicable for *in vivo* experiments. Therefore,
6 the efficiency of the system at lower power densities needs to be determined. In order to
7 enhance the cancer-targeting ability of the UCNPs, the same group developed UCNPs decorated
8 with the pH-low insertion peptide (pHLIP) which is a water-soluble membrane peptide able to
9 specifically cross the cell membrane only at slightly acidic pH.¹⁴⁷ The authors synthesised Ppa-
10 core-shell-shell NaYbF₄:Nd@NaGdF₄:Yb,Er@NaGdF₄ containing pHLIP covalently attached to the
11 UCNPs. A Ppa release of 10% was observed for pHLIP-Ppa-UCNPs stored under neutral and acidic
12 pH conditions (PBS buffer of pH 7.4 or 6.5) for 40 h.¹⁴⁷ Subsequently, the targeting ability of the
13 pHLIP-Ppa-UCNPs dissolved in PBS at pH 6.5 and 7.4 was investigated in HeLa cervical carcinoma
14 cells. Using confocal laser microscopy, higher emission intensities were observed upon 808 nm
15 excitation when the cells were incubated with pHLIP-Ppa-UCNPs at pH 6.5 indicating the
16 elevated efficiency of the pHLIP-Ppa-UCNPs to penetrate the cell membrane in an acidic
17 environment. Following the same protocol, a comparative study between pHLIP-Ppa-UCNPs and
18 NH₂-Ppa-UCNPs was performed showing higher UCNPs concentration for the pHLIP-Ppa-UCNPs
19 at pH 6.5. These results indicated that the higher efficiency of the pHLIP-Ppa-UCNPs to enter
20 cancer cells at slightly acidic pH is consequence of the pHLIP peptide functionalisation. Then, the
21 intracellular ROS production of the pHLIP-Ppa-UCNPs at both pH values was evaluated under
22 808 nm irradiation (6 W·cm⁻²) during 10 min using DCFDA as a probe. The results showed higher
23 ROS generation when HeLa cells were incubated with pHLIP-Ppa-UCNPs at pH 6.5 as expected
24 from the higher uptake at this pH. Measurements of the cell viability were performed to evaluate
25 the photo-cytotoxicity of the pHLIP-Ppa-UCNPs in HeLa cells. A significant decrease of the cell
26 viability was observed when the cells were treated with 50 µg·mL⁻¹ of pHLIP-Ppa-UCNPs at pH
27 6.5 and irradiated at 808 nm (6 W·cm⁻²) during 5 min. At this concentration, the cell viability of
28 the non-irradiated cells remained 95.2 ± 11.5%. At neutral pH conditions, a very small reduction
29 of the cell viability was observed even with 200 µg·mL⁻¹ of pHLIP-Ppa-UCNPs indicating that the
30 PDT efficiency of the pHLIP-Ppa-UCNPs increases at slightly acidic microenvironments.
31 Additionally, 4T1 cells were incubated with pHLIP-Ppa-UCNPs at pH 6.5 showing the same
32 behaviour than for HeLa cells.¹⁴⁷ *In vivo* experiments were then performed, in BALB/c mice
33 bearing 4T1 tumours, confirming the ability of the pHLIP-Ppa-UCNPs to reduce the tumour size
34 *via* PDT treatment (980 nm, 0.5 W cm⁻², 30 min).

35
36
37
38
39
40
41
42
43
44
45
46
47
48
49
50
51
52
53
54
55
56
57
58
59
60
In order to combine the targeted delivery achieved when using RGD peptide and the ability to
cross the cell membrane when functionalising nanoparticles with TAT peptide, Wang *et al.*

1
2
3 designed UCNPs modified with RGD/TAT polymeric lipid micelles and functionalised with
4 ZnPc.¹⁴¹ The authors combined three lipid proteins based on OQPGA including PEG-OQPGA,
5 RGD-OQPGA and TAT-OQPGA. The UCNPs and the ZnPc were encapsulated in the PEG-RGD-TAT-
6 OQPGA lipid micelles prepared using a thin-layer evaporation method obtaining a hydrodynamic
7 size of 82.5 nm. The encapsulation efficiency and the loading efficiency of the ZnPc into the lipid
8 micelles were evaluated showing opposite behaviour, the loading efficiency increased when
9 increasing the volume of solution containing ZnPc whereas the encapsulation efficiency
10 decreased. Additionally, leaking studies were performed showing a 50% ZnPc release after 6h
11 when then loading efficiency was 1.6%. The ability of the nanoparticles to produce ¹O₂ upon 980
12 nm excitation was confirmed using ABMA as probe.¹⁴¹ Next, the intracellular ¹O₂ production was
13 investigated in MCF-7 breast cancer cells and using DCFDA as ROS marker. The PEG-RGD-TAT-
14 OQPGA-ZnPc-UCNPs showed higher fluorescent emission intensity indicating the generation of
15 ROS. The PDT effect of PEG-RGD-TAT-OQPGA-ZnPc-UCNPs was investigated in MCF-7 cells using
16 MTS assay showing a decrease in cell viability of 85% after 980 nm excitation. A 60% cell viability
17 decrease was obtained for the nanoparticles without RGD/TAT indicating that the modification
18 of the UCNPs with RGD/TAT targeting agents allows for higher uptake of the nanoparticles. The
19 targeting capability of the nanoparticles was evaluated in B16F1 murine melanoma cells
20 overexpressing $\alpha_v\beta_3$ integrin. Cells incubated with RGD-TAT-OQPGA-ZnPc-UCNPs showed
21 stronger upconversion luminescence upon 980 nm light irradiation compared to the
22 nanoparticles without RGD peptide.¹⁴¹ Although an increased uptake of the nanoparticles by
23 cancer cells was observed for the RGD-TAT-OQPGA-ZnPc-UCNPs than for the non-modified
24 nanoparticles with targeting agents, further experiments are required to verify the actual
25 targeting ability. For instance, blocked cells with free RGD peptide previous incubation with the
26 nanoparticles, uptake comparison experiment with a negative- $\alpha_v\beta_3$ integrin cell line and *in vivo*
27 tests would confirm the potential of the RGD-TAT-OQPGA-ZnPc-UCNPs as nanosystems for
28 targeted-PDT of cancer.

29
30
31
32
33
34
35
36
37
38
39
40
41
42
43
44
45
46
47 Other peptides, such as cMBP, have shown to have targeting properties towards triple-negative
48 breast cancer (TNBC) cells compared to other cancer cells and to normal cells. With the aim of
49 applying the targeted PDT treatment to the TNBC cells, Wang *et al.* designed and synthesised
50 ZnPc@mPEG-PLGA@UCNPs (ZUPEA) using double emulsion coprecipitation method.¹⁴⁹ The
51 resulting ZUPEA nanoparticles were further functionalised with the cMBP-peptide to recognise
52 TNBC cells. Higher loading of the cMBP-ZUPEA was observed in the TNBC cells (MDA-MB-231
53 cells) compared to the normal cells (MCF-10A cells) and the MCF-7 breast cancer cell and A549
54 lung cancer cell, indicating the successful targeting of the nanoparticles to the TNBC cells. The
55
56
57
58
59
60

1
2
3 cMBP-ZUPEA exhibited good biocompatibility in normal and cancer cells and showed a great
4 cytotoxicity upon irradiation at 980 nm (1.0 W cm⁻², 10 min,). cMBP-ZUPEA were evaluated *in*
5 *vivo* in 4T1 tumour bearing mice and resulted in higher PDT effect following 980 nm irradiation
6 than when the mice were treated with ZnPc and irradiated at 650 nm. 12 days following PDT
7 treatment with the UCNPs, a significant suppression of the tumour was observed while no
8 abnormalities were observed in the organs of the treated mice.¹⁴⁹

9
10
11
12
13
14 In a recent work, Li *et al.* developed UCNPs functionalised with an antenna molecule 800CW (for
15 luminescence enhancement), RB as PS drug, Cy3 for diagnosis after treatment and cathepsin B
16 (CaB) substrate peptide labelled with QSY7 quencher for intracellular cathepsin B (CaB)-
17 responsive PDT.¹⁵⁰ The UCNPs were first functionalised with alendronic acid (ADA) to facilitate
18 the further functionalisation. Next, the 800CW dye, RB and Cy3 were immobilised on the surface
19 of the UCNPs and the CaB substrate peptide chain GRRGLGC with terminus-labelled QSY7 (Pep-
20 QSY7) was also incorporated. In the final nanosystem, the presence of the QSY7 quenches the
21 emission of the Cy3 and the RB, thus cancelling the production of ¹O₂ upon irradiation at 808 nm.
22 Upon recognition of the CaB and cleavage of the QSY7 from the UCNPs, the fluorescence
23 emission of the Cy3 is recovered and the RB is activated for the efficient PDT. The PDT effect of
24 the UCNPs in HeLa cells was evaluated by monitoring the formation of ROS with DHR and the
25 cytotoxicity with MTT assay, showing a selective and CaB concentration-dependent
26 phototoxicity. The PDT effect of the multifunctional nanosystem was evaluated *in vivo* using a
27 HeLa tumour xenograft mouse model. Antitumour efficiency was observed for mice
28 intratumorally injected with the nanoparticles (300 µg mL⁻¹) and irradiated at 808 nm (1.0 W cm⁻²,
29 40 min), which was not observed for control groups (*ie.* without UCNPs but irradiated under
30 the same conditions or injected with UCNPs but non-irradiated).¹⁵⁰

4. Conclusions

41
42
43
44
45
46
47 Based on the number of publications that report the use of PS-UCNPs for the effective treatment
48 of cancer via PDT (both *in vivo* and *in vitro*) to date, these nanosystems exhibit the potential
49 to become the next generation of nanodrugs for PDT. Further to their advantage of being NIR
50 excitable and therefore with potential for the treatment of cancers in deep-lying tissue, UCNPs
51 can accumulate in tumour tissues passively *via* the EPR effect and actively by the incorporation
52 of targeting agents to the nanoparticle surface which results in nanodrugs with reduced side
53 effects. However, despite the large body of research that has shown the viability of UCNPs for
54 PDT as an alternative to the currently used photosensitiser drugs, further improvements are
55
56
57
58
59
60

needed to bring this treatment to the clinic. Further efforts are needed to improve their biocompatibility and selectivity which would lead to improvements in therapeutic efficacy.

5. Acknowledgements

This work was supported by the Faculty of Sciences and School of Chemistry at the University of East Anglia in partnership with Mr and Mrs Whittaker oncology fellowship.

6. References

- (1) Dougherty, T. J.; Gomer, C. J.; Henderson, B. W.; Jori, G.; Kessel, D.; Korbely, M.; Moan, J.; Peng, Q. Photodynamic Therapy. *JNCI* **1998**, *90*, 889-905.
- (2) Brown, S. B.; Brown, E. A.; Walker, I. The present and future role of photodynamic therapy in cancer treatment. *Lancet Oncol.* **2004**, *5*, 497-508.
- (3) Dolmans, D. E. J. G. J.; Fukumura, D.; Jain, R. K. Photodynamic therapy for cancer. *Nat. Rev. Cancer* **2003**, *3*, 380-387.
- (4) Castano, A. P.; Demidova, T. N.; Hamblin, M. R. Mechanisms in photodynamic therapy: part one-photosensitizers, photochemistry and cellular localization. *Photodiagnosis photodyn. ther.* **2004**, *1*, 279-293.
- (5) Agostinis, P.; Berg, K.; Cengel, K. A.; Foster, T. H.; Girotti, A. W.; Gollnick, S. O.; Hahn, S. M.; Hamblin, M. R.; Juzeniene, A.; Kessel, D.; Korbely, M.; Moan, J.; Mroz, P.; Nowis, D.; Piette, J.; Wilson, B. C.; Golab, J. Photodynamic therapy of cancer: an update. *Cancer J. Clin.* **2011**, *61*, 250-281.
- (6) Kessel, D.; Oleinick, N. L. Photodynamic therapy and cell death pathways. *Methods Mol. Biol.* **2010**, *635*, 35-46.
- (7) Mroz, P.; Yaroslavsky, A.; Kharkwal, G. B.; Hamblin, M. R. Cell Death Pathways in Photodynamic Therapy of Cancer. *Cancers* **2011**, *3*, 2516-2539.
- (8) Buytaert, E.; Dewaele, M.; Agostinis, P. Molecular effectors of multiple cell death pathways initiated by photodynamic therapy. *Biochim. Biophys. Acta Rev. Cancer* **2007**, *1776*, 86-107.
- (9) Castano, A. P.; Demidova, T. N.; Hamblin, M. R. Mechanisms in photodynamic therapy: part two-cellular signaling, cell metabolism and modes of cell death. *Photodiagnosis photodyn. ther.* **2005**, *2*, 1-23.
- (10) Anand, S.; Govande, M.; Yasinchak, A.; Heusinkveld, L.; Shakya, S.; Maytin, E.: Metronomic PDT induces innate and adaptive immune responses in murine models of skin cancer and pre-cancer. *SPIE*, **2020**; *11220*.
- (11) Wu, H.; Minamide, T.; Yano, T. Role of photodynamic therapy in the treatment of esophageal cancer. *Dig. Endosc.* **2019**, *31*, 508-516.
- (12) Khan, S.; Hussain, M. A. B.; Khan, A.; Liu, H.; Siddiqui, S.; Mallidi, S.; Alacron, P.; Daly, L.; Rudd, G.; Cuckov, F.; Hopper, C.; Bown, S.; Akhtar, K.; Hasan, S. A.; Siddiqui, S. A.; Hasan, T.; Celli, J. Clinical evaluation of smartphone-based fluorescence imaging for guidance and monitoring of ALA-PDT treatment of early oral cancer. *J. Biomed. Opt.* **2020**, *25*, 1-10.

- 1
2
3
4
5
6
7
8
9
10
11
12
13
14
15
16
17
18
19
20
21
22
23
24
25
26
27
28
29
30
31
32
33
34
35
36
37
38
39
40
41
42
43
44
45
46
47
48
49
50
51
52
53
54
55
56
57
58
59
60
- (13) Usuda, J.; Inoue, T.; Tsuchida, T.; Ohtani, K.; Maehara, S.; Ikeda, N.; Ohsaki, Y.; Sasaki, T.; Oka, K. Clinical trial of photodynamic therapy for peripheral-type lung cancers using a new laser device in a pilot study. *Photodiagnosis photodyn. ther* **2020**, *30*, 101698.
- (14) Bio, M.; Rahman, K. M. M.; Lim, I.; Rajaputra, P.; Hurst, R. E.; You, Y. Singlet oxygen-activatable Paclitaxel prodrugs via intermolecular activation for combined PDT and chemotherapy. *Bioorganic Med. Chem* **2019**, *29*, 1537-1540.
- (15) Mayahi, S.; Neshasteh-Riz, A.; Pornour, M.; Eynali, S.; Montazerabadi, A. Investigation of combined photodynamic and radiotherapy effects of gallium phthalocyanine chloride on MCF-7 breast cancer cells. *J. Biol. Inorg. Chem.* **2020**, *25*, 39-48.
- (16) Montazerabadi, A. R.; Sazgarnia, A.; Bahreyni-Toosi, M. H.; Ahmadi, A.; Aledavood, A. The effects of combined treatment with ionizing radiation and indocyanine green-mediated photodynamic therapy on breast cancer cells. *J. Photochem. Photobiol. B: Biol.* **2012**, *109*, 42-49.
- (17) Biteghe, F. A. N.; Davids, L. M. A combination of photodynamic therapy and chemotherapy displays a differential cytotoxic effect on human metastatic melanoma cells. *J. Photochem. Photobiol. B: Biol.* **2017**, *166*, 18-27.
- (18) Juarranz, Á.; Jaén, P.; Sanz-Rodríguez, F.; Cuevas, J.; González, S. Photodynamic therapy of cancer. Basic principles and applications. *Clin. Transl. Oncol.* **2008**, *10*, 148-154.
- (19) Bogdan, J.; Pławińska-Czarnak, J.; Zarzyńska, J. Nanoparticles of Titanium and Zinc Oxides as Novel Agents in Tumor Treatment: a Review. *Nanoscale Res. Lett.* **2017**, *12*, 225.
- (20) Yang, F.; Liu, J.; Jiang, X.; Wu, W.; Wang, Z.; Zeng, Q.; Lv, R. Mesoporous semiconductors combined with up-conversion nanoparticles for enhanced photodynamic therapy under near infrared light. *RSC Adv.* **2019**, *9*, 17273-17280.
- (21) Borgatti-Jeffreys, A.; Hooser, S. B.; Miller, M. A.; Lucroy, M. D. Phase I clinical trial of the use of zinc phthalocyanine tetrasulfonate as a photosensitizer for photodynamic therapy in dogs. *Am. J. Vet. Res.* **2007**, *68*, 399-404.
- (22) Kato, H.; Furukawa, K.; Sato, M.; Okunaka, T.; Kusunoki, Y.; Kawahara, M.; Fukuoka, M.; Miyazawa, T.; Yana, T.; Matsui, K.; Shiraishi, T.; Horinouchi, H. Phase II clinical study of photodynamic therapy using mono-L-aspartyl chlorin e6 and diode laser for early superficial squamous cell carcinoma of the lung. *Lung Cancer* **2003**, *42*, 103-111.
- (23) Castano, A. P.; Demidova, T. N.; Hamblin, M. R. Mechanisms in photodynamic therapy: Part three-Photosensitizer pharmacokinetics, biodistribution, tumor localization and modes of tumor destruction. *Photodiagnosis photodyn. ther* **2005**, *2*, 91-106.
- (24) Ormond, A. B.; Freeman, H. S. Dye Sensitizers for Photodynamic Therapy. *Materials (Basel)* **2013**, *6*, 817-840.
- (25) Marín, M. J.; Russell, D. A.: Upconversion Nanomaterials for Photodynamic Therapy. In Near-infrared Nanomaterials: Preparation, Bioimaging and Therapy Applications. Ed. Zhang F.; Royal Society of Chemistry, Cambridge, U. K., **2016**, Chapter 7, pp. 192-231.
- (26) Chinna Ayya Swamy, P.; Sivaraman, G.; Priyanka, R. N.; Raja, S. O.; Ponnuvel, K.; Shanmugpriya, J.; Gulyani, A. Near Infrared (NIR) absorbing dyes as promising photosensitizer for photo dynamic therapy. *Coord. Chem. Rev.* **2020**, *411*, 213233.
- (27) Liu, Y.; Meng, X.; Bu, W. Upconversion-based photodynamic cancer therapy. *Coord. Chem. Rev.* **2019**, *379*, 82-98.
- (28) Obaid, G.; Russell, D. A.: Nanoparticles for Photodynamic Cancer Therapy. In Handbook of photomedicine. Ed. Hamblin, M. R., Huang, Y.-Y., Eds.; Taylor & Francis, CRC Press: Boca Raton, FL., **2013**; pp 367-378.

- 1
2
3
4
5
6
7
8
9
10
11
12
13
14
15
16
17
18
19
20
21
22
23
24
25
26
27
28
29
30
31
32
33
34
35
36
37
38
39
40
41
42
43
44
45
46
47
48
49
50
51
52
53
54
55
56
57
58
59
60
- (29) Singh, R.; Lillard, J. W., Jr. Nanoparticle-based targeted drug delivery. *Exp. Mol. Pathol.* **2009**, *86*, 215-223.
- (30) Fang, J.; Nakamura, H.; Maeda, H. The EPR effect: Unique features of tumor blood vessels for drug delivery, factors involved, and limitations and augmentation of the effect. *Adv. Drug Deliv. Rev.* **2011**, *63*, 136-151.
- (31) Iyer, A. K.; Khaled, G.; Fang, J.; Maeda, H. Exploiting the enhanced permeability and retention effect for tumor targeting. *Drug Discov. Today* **2006**, *11*, 812-818.
- (32) Yi, G.; Hong, S. H.; Son, J.; Yoo, J.; Park, C.; Choi, Y.; Koo, H. Recent advances in nanoparticle carriers for photodynamic therapy. *Quant. Imaging Med. Surg.* **2018**, *8*, 433-443.
- (33) Duse, L.; Agel, M. R.; Pinnapireddy, S. R.; Schäfer, J.; Selo, M. A.; Ehrhardt, C.; Bakowsky, U. Photodynamic Therapy of Ovarian Carcinoma Cells with Curcumin-Loaded Biodegradable Polymeric Nanoparticles. *Pharmaceutics* **2019**, *11*, 282.
- (34) Ghosh, S.; Carter, K. A.; Lovell, J. F. Liposomal formulations of photosensitizers. *Biomaterials* **2019**, *218*, 119341.
- (35) Bretin, L.; Leger, D.-Y.; Pinon, A.; Bouramtane, S.; Bregier, F.; Sol, V.; Chaleix, V.; Liagre, B.: Photodynamic therapy activity of new porphyrin-xylan-coated silica nanoparticles in a human colorectal cancer in vivo model. *SPIE*, **2019**, 11070.
- (36) Camerin, M.; Moreno, M.; Marín, M. J.; Schofield, C. L.; Chambrier, I.; Cook, M. J.; Coppellotti, O.; Jori, G.; Russell, D. A. Delivery of a hydrophobic phthalocyanine photosensitizer using PEGylated gold nanoparticle conjugates for the in vivo photodynamic therapy of amelanotic melanoma. *Photochem. Photobiol. Sci.* **2016**, *15*, 618-625.
- (37) García Calavia, P.; Marín, M. J.; Chambrier, I.; Cook, M. J.; Russell, D. A. Towards optimisation of surface enhanced photodynamic therapy of breast cancer cells using gold nanoparticle–photosensitiser conjugates. *Photochem. Photobiol. Sci.* **2018**, *17*, 281-289.
- (38) Goddard, Z. R.; Marín, M. J.; Russell, D. A.; Searcey, M. Active targeting of gold nanoparticles as cancer therapeutics. *Chem. Soc. Rev.* **2020**, *49*, 8774-8789.
- (39) Goddard, Z. R.; Beekman, A. M.; Cominetti, M. M. D.; O'Connell, M. A.; Chambrier, I.; Cook, M. J.; Marín, M. J.; Russell, D. A.; Searcey, M. Peptide directed phthalocyanine–gold nanoparticles for selective photodynamic therapy of EGFR overexpressing cancers. *RSC Med. Chem.* **2021**, *12*, 288-292.
- (40) Rivas Aiello, M. B.; Castrogiovanni, D.; Parisi, J.; Azcárate, J. C.; García Einschlag, F. S.; Gensch, T.; Bosio, G. N.; Mártire, D. O. Photodynamic Therapy in HeLa Cells Incubated with Riboflavin and Pectin-coated Silver Nanoparticles. *Photochem. Photobiol.* **2018**, *94*, 1159-1166.
- (41) Penon, O.; Marín, M. J.; Amabilino, D. B.; Russell, D. A.; Pérez-García, L. Iron oxide nanoparticles functionalized with novel hydrophobic and hydrophilic porphyrins as potential agents for photodynamic therapy. *J. Colloid Interface Sci.* **2016**, *462*, 154-165.
- (42) Wang, D.; Fei, B.; Halig, L. V.; Qin, X.; Hu, Z.; Xu, H.; Wang, Y. A.; Chen, Z.; Kim, S.; Shin, D. M.; Chen, Z. G. Targeted iron-oxide nanoparticle for photodynamic therapy and imaging of head and neck cancer. *ACS Nano* **2014**, *8*, 6620-6632.
- (43) Wang, S.; Huang, P.; Nie, L.; Xing, R.; Liu, D.; Wang, Z.; Lin, J.; Chen, S.; Niu, G.; Lu, G.; Chen, X. Single Continuous Wave Laser Induced Photodynamic/Plasmonic Photothermal Therapy Using Photosensitizer-Functionalized Gold Nanostars. *Adv. Mater.* **2013**, *25*, 3055-3061.

- 1
2
3
4
5
6
7
8
9
10
11
12
13
14
15
16
17
18
19
20
21
22
23
24
25
26
27
28
29
30
31
32
33
34
35
36
37
38
39
40
41
42
43
44
45
46
47
48
49
50
51
52
53
54
55
56
57
58
59
60
- (44) Lee, S. J.; Koo, H.; Jeong, H.; Huh, M. S.; Choi, Y.; Jeong, S. Y.; Byun, Y.; Choi, K.; Kim, K.; Kwon, I. C. Comparative study of photosensitizer loaded and conjugated glycol chitosan nanoparticles for cancer therapy. *J. Control. Release* **2011**, *152*, 21-29.
- (45) Alea-Reyes, M. E.; Rodrigues, M.; Serrà, A.; Mora, M.; Sagristá, M. L.; González, A.; Durán, S.; Duch, M.; Plaza, J. A.; Vallés, E.; Russell, D. A.; Pérez-García, L. Nanostructured materials for photodynamic therapy: synthesis, characterization and in vitro activity. *RSC Adv.* **2017**, *7*, 16963-16976.
- (46) Brandhonneur, N.; Hatahet, T.; Amela-Cortes, M.; Molard, Y.; Cordier, S.; Dollo, G. Molybdenum cluster loaded PLGA nanoparticles: An innovative theranostic approach for the treatment of ovarian cancer. *Eur. J. Pharm. Biopharm.* **2018**, *125*, 95-105.
- (47) Almeida, J. P. M.; Chen, A. L.; Foster, A.; Drezek, R. In vivo biodistribution of nanoparticles. *Nanomedicine (Lond.)* **2011**, *6*, 815-835.
- (48) Penon, O.; Marín, M. J.; Russell, D. A.; Pérez-García, L. Water soluble, multifunctional antibody-porphyrin gold nanoparticles for targeted photodynamic therapy. *J. Colloid Interface Sci.* **2017**, *496*, 100-110.
- (49) Samia, A. C. S.; Chen, X.; Burda, C. Semiconductor Quantum Dots for Photodynamic Therapy. *J. Am. Chem. Soc.* **2003**, *125*, 15736-15737.
- (50) Fan, H.-y.; Yu, X.-h.; Wang, K.; Yin, Y.-j.; Tang, Y.-j.; Tang, Y.-l.; Liang, X.-h. Graphene quantum dots (GQDs)-based nanomaterials for improving photodynamic therapy in cancer treatment. *Eur. J. Med. Chem.* **2019**, *182*, 111620.
- (51) Buchner, M.; García Calavia, P.; Muhr, V.; Kröninger, A.; Baeumner, A. J.; Hirsch, T.; Russell, D. A.; Marín, M. J. Photosensitiser functionalised luminescent upconverting nanoparticles for efficient photodynamic therapy of breast cancer cells. *Photochem. Photobiol. Sci.* **2019**, *18*, 98 - 109.
- (52) Chatterjee, D. K.; Yong, Z. Upconverting nanoparticles as nanotransducers for photodynamic therapy in cancer cells. *Nanomedicine* **2008**, *3*, 73-82.
- (53) Hou, W.; Liu, Y.; Jiang, Y.; Wu, Y.; Cui, C.; Wang, Y.; Zhang, L.; Teng, I. T.; Tan, W. Aptamer-based multifunctional ligand-modified UCNPs for targeted PDT and bioimaging. *Nanoscale* **2018**, *10*, 10986-10990.
- (54) Chatterjee, D. K.; Fong, L. S.; Zhang, Y. Nanoparticles in photodynamic therapy: An emerging paradigm. *Adv. Drug Deliv. Rev.* **2008**, *60*, 1627-1637.
- (55) Wang, C.; Cheng, L.; Liu, Z. Upconversion nanoparticles for photodynamic therapy and other cancer therapeutics. *Theranostics* **2013**, *3*, 317-330.
- (56) Haase, M.; Schäfer, H. Upconverting Nanoparticles. *Angew. Chem. Int. Ed.* **2011**, *50*, 5808-5829.
- (57) Li, K.; Hong, E.; Wang, B.; Wang, Z.; Zhang, L.; Hu, R.; Wang, B. Advances in the application of upconversion nanoparticles for detecting and treating cancers. *Photodiagnosis Photodyn. Ther.* **2019**, *25*, 177-192.
- (58) Wen, S.; Zhou, J.; Zheng, K.; Bednarkiewicz, A.; Liu, X.; Jin, D. Advances in highly doped upconversion nanoparticles. *Nat. Commun.* **2018**, *9*, 2415.
- (59) Mandl, G. A.; Cooper, D. R.; Hirsch, T.; Seuntjens, J.; Capobianco, J. A. Perspective: lanthanide-doped upconverting nanoparticles. *Methods Appl. Fluoresc.* **2019**, *7*, 012004.
- (60) Wilhelm, S.; Hirsch, T.; Patterson, W. M.; Scheucher, E.; Mayr, T.; Wolfbeis, O. S. Multicolor upconversion nanoparticles for protein conjugation. *Theranostics* **2013**, *3*, 239-248.
- (61) Boyer, J.-C.; Vetrone, F.; Cuccia, L. A.; Capobianco, J. A. Synthesis of Colloidal Upconverting NaYF₄ Nanocrystals Doped with Er³⁺, Yb³⁺ and Tm³⁺, Yb³⁺ via Thermal

- Decomposition of Lanthanide Trifluoroacetate Precursors. *J. Am. Chem. Soc.* **2006**, *128*, 7444-7445.
- (62) Wang, M.; Abbineni, G.; Clevenger, A.; Mao, C.; Xu, S. Upconversion nanoparticles: synthesis, surface modification and biological applications. *Nanomed.: Nanotechnol. Biol. Med.* **2011**, *7*, 710-729.
- (63) Xiong, L.; Chen, Z.; Tian, Q.; Cao, T.; Xu, C.; Li, F. High Contrast Upconversion Luminescence Targeted Imaging in Vivo Using Peptide-Labeled Nanophosphors. *Anal. Chem.* **2009**, *81*, 8687-8694.
- (64) Bogdan, N.; Vetrone, F.; Roy, R.; Capobianco, J. A. Carbohydrate-coated lanthanide-doped upconverting nanoparticles for lectin recognition. *J. Mater. Chem.* **2010**, *20*, 7543-7550.
- (65) Xiong, L.-Q.; Chen, Z.-G.; Yu, M.-X.; Li, F.-Y.; Liu, C.; Huang, C.-H. Synthesis, characterization, and in vivo targeted imaging of amine-functionalized rare-earth upconverting nanophosphors. *Biomaterials* **2009**, *30*, 5592-5600.
- (66) Wang, M.; Mi, C.-C.; Wang, W.-X.; Liu, C.-H.; Wu, Y.-F.; Xu, Z.-R.; Mao, C.-B.; Xu, S.-K. Immunolabeling and NIR-Excited Fluorescent Imaging of HeLa Cells by Using NaYF₄:Yb,Er Upconversion Nanoparticles. *ACS Nano* **2009**, *3*, 1580-1586.
- (67) Wang, N.; Yu, X.; Zhang, K.; Mirkin, C. A.; Li, J. Upconversion Nanoprobes for the Ratiometric Luminescent Sensing of Nitric Oxide. *J. Am. Chem. Soc.* **2017**, *139*, 12354-12357.
- (68) Cui, S.; Chen, H.; Zhu, H.; Tian, J.; Chi, X.; Qian, Z.; Achilefu, S.; Gu, Y. Amphiphilic chitosan modified upconversion nanoparticles for in vivo photodynamic therapy induced by near-infrared light. *J. Mater. Chem.* **2012**, *22*, 4861-4873.
- (69) DaCosta, M. V.; Doughan, S.; Han, Y.; Krull, U. J. Lanthanide upconversion nanoparticles and applications in bioassays and bioimaging: A review. *Anal. Chim. Acta* **2014**, *832*, 1-33.
- (70) Haase, M.; Schäfer, H. Upconverting Nanoparticles. *Angew. Chem. Int. Ed.* **2011**, *50*, 5808-5829.
- (71) Gnach, A.; Lipinski, T.; Bednarkiewicz, A.; Rybka, J.; Capobianco, J. A. Upconverting nanoparticles: assessing the toxicity. *Chem. Soc. Rev.* **2015**, *44*, 1561-1584.
- (72) Zhang, P.; Steelant, W.; Kumar, M.; Scholfield, M. Versatile Photosensitizers for Photodynamic Therapy at Infrared Excitation. *J. Am. Chem. Soc.* **2007**, *129*, 4526-4527.
- (73) Guo, Y.; Kumar, M.; Zhang, P. Nanoparticle-Based Photosensitizers under CW Infrared Excitation. *Chem. Mater.* **2007**, *19*, 6071-6072.
- (74) Qiu, H.; Tan, M.; Ohulchanskyy, T. Y.; Lovell, J. F.; Chen, G. Recent Progress in Upconversion Photodynamic Therapy. *Nanomaterials (Basel)* **2018**, *8*, 344.
- (75) Cheng, L.; Wang, C.; Liu, Z. Upconversion nanoparticles and their composite nanostructures for biomedical imaging and cancer therapy. *Nanoscale* **2013**, *5*, 23-37.
- (76) Qian, H. S.; Guo, H. C.; Ho, P. C.-L.; Mahendran, R.; Zhang, Y. Mesoporous-Silica-Coated Up-Conversion Fluorescent Nanoparticles for Photodynamic Therapy. *Small* **2009**, *5*, 2285-2290.
- (77) Guo, H.; Qian, H.; Idris, N. M.; Zhang, Y. Singlet oxygen-induced apoptosis of cancer cells using upconversion fluorescent nanoparticles as a carrier of photosensitizer. *Nanomed.: Nanotechnol. Biol. Med.* **2010**, *6*, 486-495.
- (78) Wang, D.; Xue, B.; Kong, X.; Tu, L.; Liu, X.; Zhang, Y.; Chang, Y.; Luo, Y.; Zhao, H.; Zhang, H. 808 nm driven Nd³⁺-sensitized upconversion nanostructures for photodynamic therapy and simultaneous fluorescence imaging. *Nanoscale* **2015**, *7*, 190-197.

- 1
2
3
4
5
6
7
8
9
10
11
12
13
14
15
16
17
18
19
20
21
22
23
24
25
26
27
28
29
30
31
32
33
34
35
36
37
38
39
40
41
42
43
44
45
46
47
48
49
50
51
52
53
54
55
56
57
58
59
60
- (79) Sabri, T.; Pawelek, P. D.; Capobianco, J. A. Dual Activity of Rose Bengal Functionalized to Albumin-Coated Lanthanide-Doped Upconverting Nanoparticles: Targeting and Photodynamic Therapy. *ACS Appl. Mater. Interfaces* **2018**, *10*, 26947-26953.
- (80) Arias, J. L. Drug Targeting Strategies in Cancer Treatment: An Overview. *Mini Rev. Med. Chem.* **2011**, *11*, 1-17.
- (81) Sharma, P.; Brown, S.; Walter, G.; Santra, S.; Moudgil, B. Nanoparticles for bioimaging. *Adv. Colloid Interface Sci.* **2006**, *123-126*, 471-485.
- (82) Xie, J.; Lee, S.; Chen, X. Nanoparticle-based theranostic agents. *Adv. Drug Deliv. Rev.* **2010**, *62*, 1064-1079.
- (83) Han, R.; Shi, J.; Liu, Z.; Wang, H.; Wang, Y. Fabrication of Mesoporous-Silica-Coated Upconverting Nanoparticles with Ultrafast Photosensitizer Loading and 808 nm NIR-Light-Triggering Capability for Photodynamic Therapy. *Chem. Asian J.* **2017**, *12*, 2197-2201.
- (84) Wang, H.; Han, R.-l.; Yang, L.-m.; Shi, J.-h.; Liu, Z.-j.; Hu, Y.; Wang, Y.; Liu, S.-j.; Gan, Y. Design and Synthesis of Core-Shell-Shell Upconversion Nanoparticles for NIR-Induced Drug Release, Photodynamic Therapy, and Cell Imaging. *ACS Appl. Mater. Interfaces* **2016**, *8*, 4416-4423.
- (85) Xu, F.; Ding, L.; Tao, W.; Yang, X.-z.; Qian, H.-s.; Yao, R.-s. Mesoporous-silica-coated upconversion nanoparticles loaded with vitamin B12 for near-infrared-light mediated photodynamic therapy. *Mater. Lett.* **2016**, *167*, 205-208.
- (86) Wang, C.; Tao, H.; Cheng, L.; Liu, Z. Near-infrared light induced in vivo photodynamic therapy of cancer based on upconversion nanoparticles. *Biomaterials* **2011**, *32*, 6145-6154.
- (87) Meng, Z.; Zhang, L.; He, Z.; Lian, H. Mucosal Penetrating Bioconjugate Coated Upconverting Nanoparticles That Integrate Biological Tracking and Photodynamic Therapy for Gastrointestinal Cancer Treatment. *ACS Biomater. Sci. Eng.* **2018**, *4*, 2203-2212.
- (88) Liu, X.; Qian, H.; Ji, Y.; Li, Z.; Shao, Y.; Hu, Y.; Tong, G.; Li, L.; Guo, W.; Guo, H. Mesoporous silica-coated NaYF₄ nanocrystals: facile synthesis, in vitro bioimaging and photodynamic therapy of cancer cells. *RSC Adv.* **2012**, *2*, 12263-12268.
- (89) Wang, C.; Cheng, L.; Liu, Y.; Wang, X.; Ma, X.; Deng, Z.; Li, Y.; Liu, Z. Imaging-Guided pH-Sensitive Photodynamic Therapy Using Charge Reversible Upconversion Nanoparticles under Near-Infrared Light. *Adv. Funct. Mater.* **2013**, *23*, 3077-3086.
- (90) Liu, K.; Liu, X.; Zeng, Q.; Zhang, Y.; Tu, L.; Liu, T.; Kong, X.; Wang, Y.; Cao, F.; Lambrechts, S. A. G.; Aalders, M. C. G.; Zhang, H. Covalently Assembled NIR NanoplatforM for Simultaneous Fluorescence Imaging and Photodynamic Therapy of Cancer Cells. *ACS Nano* **2012**, *6*, 4054-4062.
- (91) Wang, M.; Chen, Z.; Zheng, W.; Zhu, H.; Lu, S.; Ma, E.; Tu, D.; Zhou, S.; Huang, M.; Chen, X. Lanthanide-doped upconversion nanoparticles electrostatically coupled with photosensitizers for near-infrared-triggered photodynamic therapy. *Nanoscale* **2014**, *6*, 8274-8282.
- (92) Muhr, V.; Würth, C.; Kraft, M.; Buchner, M.; Baeumner, A. J.; Resch-Genger, U.; Hirsch, T. Particle-Size-Dependent Förster Resonance Energy Transfer from Upconversion Nanoparticles to Organic Dyes. *Anal. Chem.* **2017**, *89*, 4868-4874.
- (93) Sun, X.; Zhang, P.; Hou, Y.; Li, Y.; Huang, X.; Wang, Z.; Jing, L.; Gao, M. Upconversion luminescence mediated photodynamic therapy through hydrophilically engineered porphyrin. *Chem. Eng. Process.* **2019**, *142*, 107551.

- 1
2
3
4
5
6
7
8
9
10
11
12
13
14
15
16
17
18
19
20
21
22
23
24
25
26
27
28
29
30
31
32
33
34
35
36
37
38
39
40
41
42
43
44
45
46
47
48
49
50
51
52
53
54
55
56
57
58
59
60
- (94) Ritz, S.; Schöttler, S.; Kotman, N.; Baier, G.; Musyanovych, A.; Kuharev, J.; Landfester, K.; Schild, H.; Jahn, O.; Tenzer, S.; Mailänder, V. Protein Corona of Nanoparticles: Distinct Proteins Regulate the Cellular Uptake. *Biomacromolecules* **2015**, *16*, 1311-1321.
- (95) Gao, W.; Zhang, L. Coating nanoparticles with cell membranes for targeted drug delivery. *J. Drug Target.* **2015**, *23*, 619-626.
- (96) Georgakoudi, I.; Nichols, M. G.; Foster, T. H. The mechanism of Photofrin photobleaching and its consequences for photodynamic dosimetry. *Photochem. Photobiol.* **1997**, *65*, 135-144.
- (97) Gao, C.; Lin, Z.; Wu, Z.; Lin, X.; He, Q. Stem-Cell-Membrane Camouflaging on Near-Infrared Photoactivated Upconversion Nanoarchitectures for in Vivo Remote-Controlled Photodynamic Therapy. *ACS Appl. Mater. Interfaces* **2016**, *8*, 34252-34260.
- (98) Dou, Q. Q.; Rengaramchandran, A.; Selvan, S. T.; Paulmurugan, R.; Zhang, Y. Core-shell upconversion nanoparticle – semiconductor heterostructures for photodynamic therapy. *Sci. Rep.* **2015**, *5*, 8252.
- (99) Lucky, S. S.; Muhammad Idris, N.; Li, Z.; Huang, K.; Soo, K. C.; Zhang, Y. Titania Coated Upconversion Nanoparticles for Near-Infrared Light Triggered Photodynamic Therapy. *ACS Nano* **2015**, *9*, 191-205.
- (100) Hou, Z.; Zhang, Y.; Deng, K.; Chen, Y.; Li, X.; Deng, X.; Cheng, Z.; Lian, H.; Li, C.; Lin, J. UV-Emitting Upconversion-Based TiO₂ Photosensitizing Nanoplatform: Near-Infrared Light Mediated in Vivo Photodynamic Therapy via Mitochondria-Involved Apoptosis Pathway. *ACS Nano* **2015**, *9*, 2584-2599.
- (101) Zhao, J.; Sun, S.; Li, X.; Zhang, W.; Gou, S. Enhancing Photodynamic Therapy Efficacy of Upconversion-Based Nanoparticles Conjugated with a Long-Lived Triplet Excited State Iridium(III)-Naphthalimide Complex: Toward Highly Enhanced Hypoxia-Inducible Factor-1. *ACS Appl. Bio Mater.* **2020**, *3*, 252-262.
- (102) Meijer, M. S.; Talens, V. S.; Hilbers, M. F.; Kieltyka, R. E.; Brouwer, A. M.; Natile, M. M.; Bonnet, S. NIR-Light-Driven Generation of Reactive Oxygen Species Using Ru(II)-Decorated Lipid-Encapsulated Upconverting Nanoparticles. *Langmuir* **2019**, *35*, 12079-12090.
- (103) Shi, Z.; Zhang, K.; Zada, S.; Zhang, C.; Meng, X.; Yang, Z.; Dong, H. Upconversion Nanoparticle-Induced Multimode Photodynamic Therapy Based on a Metal-Organic Framework/Titanium Dioxide Nanocomposite. *ACS Appl. Mater. Interfaces* **2020**, *12*, 12600-12608.
- (104) Jia, T.; Xu, J.; Dong, S.; He, F.; Zhong, C.; Yang, G.; Bi, H.; Xu, M.; Hu, Y.; Yang, D.; Yang, P.; Lin, J. Mesoporous cerium oxide-coated upconversion nanoparticles for tumor-responsive chemo-photodynamic therapy and bioimaging. *Chem. Sci.* **2019**, *10*, 8618-8633.
- (105) Feng, Y.; Chen, H.; Wu, Y.; Que, I.; Tamburini, F.; Baldazzi, F.; Chang, Y.; Zhang, H. Optical imaging and pH-awakening therapy of deep tissue cancer based on specific upconversion nanophotosensitizers. *Biomaterials* **2020**, *230*, 119637.
- (106) Punjabi, A.; Wu, X.; Tokatli-Apollon, A.; El-Rifai, M.; Lee, H.; Zhang, Y.; Wang, C.; Liu, Z.; Chan, E. M.; Duan, C.; Han, G. Amplifying the Red-Emission of Upconverting Nanoparticles for Biocompatible Clinically Used Prodrug-Induced Photodynamic Therapy. *ACS Nano* **2014**, *8*, 10621-10630.
- (107) Ding, B.; Shao, S.; Xiao, H.; Sun, C.; Cai, X.; Jiang, F.; Zhao, X.; Ma, P. a.; Lin, J. MnFe₂O₄-decorated large-pore mesoporous silica-coated upconversion nanoparticles for near-

- infrared light-induced and O₂ self-sufficient photodynamic therapy. *Nanoscale* **2019**, *11*, 14654-14667.
- (108) Kumar, B.; Murali, A.; Bharath, A. B.; Giri, S. Guar gum modified upconversion nanocomposites for colorectal cancer treatment through enzyme-responsive drug release and NIR-triggered photodynamic therapy. *Nanotechnology* **2019**, *30*, 315102.
- (109) Mahmoudi, K.; Garvey, K. L.; Bouras, A.; Cramer, G.; Stepp, H.; Jesu Raj, J. G.; Bozec, D.; Busch, T. M.; Hadjipanayis, C. G. 5-aminolevulinic acid photodynamic therapy for the treatment of high-grade gliomas. *J. Neuro-Oncol.* **2019**, *141*, 595-607.
- (110) Liou, G.-Y.; Storz, P. Reactive oxygen species in cancer. *Free Radic. Res.* **2010**, *44*, 479-496.
- (111) Hu, J.; Shi, J.; Gao, Y.; Yang, W.; Liu, P.; Liu, Q.; He, F.; Wang, C.; Li, T.; Xie, R.; Zhu, J.; Yang, P. 808 nm Near-Infrared Light-Excited UCNPs@mSiO₂-Ce6-GPC3 Nanocomposites For Photodynamic Therapy In Liver Cancer. *Int. J. Nanomedicine* **2019**, *14*, 10009-10021.
- (112) García Calavia, P.; Chambrier, I.; Cook, M. J.; Haines, A. H.; Field, R. A.; Russell, D. A. Targeted photodynamic therapy of breast cancer cells using lactose-phthalocyanine functionalized gold nanoparticles. *J. Colloid Interface Sci.* **2018**, *512*, 249-259.
- (113) Wang, D.; Zhu, L.; Pu, Y.; Wang, J.-X.; Chen, J.-F.; Dai, L. Transferrin-coated magnetic upconversion nanoparticles for efficient photodynamic therapy with near-infrared irradiation and luminescence bioimaging. *Nanoscale* **2017**, *9*, 11214-11221.
- (114) Scott, A. M.; Allison, J. P.; Wolchok, J. D. Monoclonal antibodies in cancer therapy. *Cancer Immun. Archive* **2012**, *12*, 14.
- (115) Liang, L.; Care, A.; Zhang, R.; Lu, Y.; Packer, N. H.; Sunna, A.; Qian, Y.; Zvyagin, A. V. Facile Assembly of Functional Upconversion Nanoparticles for Targeted Cancer Imaging and Photodynamic Therapy. *ACS Appl. Mater. Interfaces* **2016**, *8*, 11945-11953.
- (116) Ramírez-García, G.; Panikar, S. S.; López-Luke, T.; Piazza, V.; Honorato-Colin, M. A.; Camacho-Villegas, T.; Hernández-Gutiérrez, R.; De la Rosa, E. An immunconjugated up-conversion nanocomplex for selective imaging and photodynamic therapy against HER2-positive breast cancer. *Nanoscale* **2018**, *10*, 10154-10165.
- (117) Sigismund, S.; Avanzato, D.; Lanzetti, L. Emerging functions of the EGFR in cancer. *Mol. Oncol.* **2018**, *12*, 3-20.
- (118) Lucky, S. S.; Idris, N. M.; Huang, K.; Kim, J.; Li, Z.; Thong, P. S. P.; Xu, R.; Soo, K. C.; Zhang, Y. In vivo Biocompatibility, Biodistribution and Therapeutic Efficiency of Titania Coated Upconversion Nanoparticles for Photodynamic Therapy of Solid Oral Cancers. *Theranostics* **2016**, *6*, 1844-1865.
- (119) Leamon, C. P.; Vlahov, I. R.; Reddy, J. A.; Vetzal, M.; Santhapuram, H. K. R.; You, F.; Bloomfield, A.; Dorton, R.; Nelson, M.; Kleindl, P.; Vaughn, J. F.; Westrick, E. Folate-Vinca Alkaloid Conjugates for Cancer Therapy: A Structure-Activity Relationship. *Bioconjugate Chem.* **2014**, *25*, 560-568.
- (120) Fernández, M.; Javid, F.; Chudasama, V. Advances in targeting the folate receptor in the treatment/imaging of cancers. *Chem. Sci.* **2018**, *9*, 790-810.
- (121) Ai, F.; Ju, Q.; Zhang, X.; Chen, X.; Wang, F.; Zhu, G. A core-shell-shell nanoplatform upconverting near-infrared light at 808 nm for luminescence imaging and photodynamic therapy of cancer. *Sci. Rep.* **2015**, *5*, 10785-10785.
- (122) Thanasekaran, P.; Chu, C.-H.; Wang, S.-B.; Chen, K.-Y.; Gao, H.-D.; Lee, M. M.; Sun, S.-S.; Li, J.-P.; Chen, J.-Y.; Chen, J.-K.; Chang, Y.-H.; Lee, H.-M. Lipid-Wrapped Upconversion

- Nanoconstruct/Photosensitizer Complex for Near-Infrared Light-Mediated Photodynamic Therapy. *ACS Appl. Mater. Interfaces* **2019**, *11*, 84-95.
- (123) Wang, F.; Yang, X.; Ma, L.; Huang, B.; Na, N.; E, Y.; He, D.; Ouyang, J. Multifunctional up-converting nanocomposites with multimodal imaging and photosensitization at near-infrared excitation. *J. Mater. Chem.* **2012**, *22*, 24597-24604.
- (124) Yang, X.; Xiao, Q.; Niu, C.; Jin, N.; Ouyang, J.; Xiao, X.; He, D. Multifunctional core-shell upconversion nanoparticles for targeted tumor cells induced by near-infrared light. *J. Mater. Chem. B* **2013**, *1*, 2757-2763.
- (125) Idris, N. M.; Gnanasammandhan, M. K.; Zhang, J.; Ho, P. C.; Mahendran, R.; Zhang, Y. In vivo photodynamic therapy using upconversion nanoparticles as remote-controlled nanotransducers. *Nat. Med.* **2012**, *18*, 1580.
- (126) Wang, H.; Liu, Z.; Wang, S.; Dong, C.; Gong, X.; Zhao, P.; Chang, J. MC540 and Upconverting Nanocrystal Coloaded Polymeric Liposome for Near-Infrared Light-Triggered Photodynamic Therapy and Cell Fluorescent Imaging. *ACS Appl. Mater. Interfaces* **2014**, *6*, 3219-3225.
- (127) Cui, S.; Yin, D.; Chen, Y.; Di, Y.; Chen, H.; Ma, Y.; Achilefu, S.; Gu, Y. In Vivo Targeted Deep-Tissue Photodynamic Therapy Based on Near-Infrared Light Triggered Upconversion Nanoconstruct. *ACS Nano* **2013**, *7*, 676-688.
- (128) Liu, X.; Zheng, M.; Kong, X.; Zhang, Y.; Zeng, Q.; Sun, Z.; Buma, W. J.; Zhang, H. Separately doped upconversion-C60 nanoplatfor for NIR imaging-guided photodynamic therapy of cancer cells. *Chem. Comm.* **2013**, *49*, 3224-3226.
- (129) Xia, L.; Kong, X.; Liu, X.; Tu, L.; Zhang, Y.; Chang, Y.; Liu, K.; Shen, D.; Zhao, H.; Zhang, H. An upconversion nanoparticle – Zinc phthalocyanine based nanophotosensitizer for photodynamic therapy. *Biomaterials* **2014**, *35*, 4146-4156.
- (130) Liu, X.; Que, I.; Kong, X.; Zhang, Y.; Tu, L.; Chang, Y.; Wang, T. T.; Chan, A.; Löwik, C. W. G. M.; Zhang, H. In vivo 808 nm image-guided photodynamic therapy based on an upconversion theranostic nanoplatfor. *Nanoscale* **2015**, *7*, 14914-14923.
- (131) Yu, Z.; Ge, Y.; Sun, Q.; Pan, W.; Wan, X.; Li, N.; Tang, B. A pre-protective strategy for precise tumor targeting and efficient photodynamic therapy with a switchable DNA/upconversion nanocomposite. *Chem. Sci.* **2018**, *9*, 3563-3569.
- (132) Song, X.; Yue, Z.; Hong, T.; Wang, Z.; Zhang, S. Sandwich-Structured Upconversion Nanoprobes Coated with a Thin Silica Layer for Mitochondria-Targeted Cooperative Photodynamic Therapy for Solid Malignant Tumors. *Anal. Chem.* **2019**, *91*, 8549-8557.
- (133) Zhao, L.; Choi, J.; Lu, Y.; Kim, S. Y. NIR Photoregulated Theranostic System Based on Hexagonal-Phase Upconverting Nanoparticles for Tumor-Targeted Photodynamic Therapy and Fluorescence Imaging. *Nanomaterials* **2020**, *10*, 2332.
- (134) Lim, K.; Kim, H. K.; Le, X. T.; Nguyen, N. T.; Lee, E. S.; Oh, K. T.; Choi, H.-G.; Youn, Y. S. Highly Red Light-Emitting Erbium- and Lutetium-Doped Core-Shell Upconverting Nanoparticles Surface-Modified with PEG-Folic Acid/TCPP for Suppressing Cervical Cancer HeLa Cells. *Pharmaceutics* **2020**, *12*, 1102.
- (135) Daniels, T. R.; Bernabeu, E.; Rodríguez, J. A.; Patel, S.; Kozman, M.; Chiappetta, D. A.; Holler, E.; Ljubimova, J. Y.; Helguera, G.; Penichet, M. L. The transferrin receptor and the targeted delivery of therapeutic agents against cancer. *Biochim. Biophys. Acta Gen. Subj.* **2012**, *1820*, 291-317.
- (136) Liu, S.; Yuan, Y.; Yang, Y.; Liu, Z.; Yin, S.; Qin, W.; Wu, C. Multilayered upconversion nanocomposites with dual photosensitizing functions for enhanced photodynamic therapy. *J. Mater. Chem. B* **2017**, *5*, 8169-8177.

- 1
2
3 (137) Zhang, T.; Lin, H.; Cui, L.; An, N.; Tong, R.; Chen, Y.; Yang, C.; Li, X.; Qu, F. NIR-sensitive
4 UCNP@mSiO₂ nanovehicles for on-demand drug release and photodynamic therapy.
5 *RSC Adv.* **2016**, *6*, 26479-26489.
6
7 (138) Zhang, T.; Huang, S.; Lin, H.; An, N.; Tong, R.; Chen, Y.; Wang, Y.; Qu, F. Enzyme and pH-
8 responsive nanovehicles for intracellular drug release and photodynamic therapy. *New*
9 *J. Chem.* **2017**, *41*, 2468-2478.
10
11 (139) Raha, S.; Paunesku, T.; Woloschak, G. Peptide-mediated cancer targeting of
12 nanoconjugates. *Wiley Interdiscip. Rev. Nanomed. Nanobiotechnol.* **2011**, *3*, 269-281.
13
14 (140) Torchilin, V. P. Tat peptide-mediated intracellular delivery of pharmaceutical
15 nanocarriers. *Adv. Drug Deliv. Rev.* **2008**, *60*, 548-558.
16
17 (141) Wang, H. J.; Shrestha, R.; Zhang, Y. Encapsulation of Photosensitizers and Upconversion
18 Nanocrystals in Lipid Micelles for Photodynamic Therapy. *Part. Part. Syst. Charact.* **2014**,
19 *31*, 228-235.
20
21 (142) Zhang, X.; Ai, F.; Sun, T.; Wang, F.; Zhu, G. Multimodal Upconversion Nanoplatfom with
22 a Mitochondria-Targeted Property for Improved Photodynamic Therapy of Cancer Cells.
23 *Inorg. Chem.* **2016**, *55*, 3872-3880.
24
25 (143) Roveri, M.; Bernasconi, M.; Leroux, J.-C.; Luciani, P. Peptides for tumor-specific drug
26 targeting: state of the art and beyond. *J. Mater. Chem. B* **2017**, *5*, 4348-4364.
27
28 (144) Wang, H.; Dong, C.; Zhao, P.; Wang, S.; Liu, Z.; Chang, J. Lipid coated upconverting
29 nanoparticles as NIR remote controlled transducer for simultaneous photodynamic
30 therapy and cell imaging. *Int. J. Pharm.* **2014**, *466*, 307-313.
31
32 (145) Hou, B.; Zheng, B.; Gong, X.; Wang, H.; Wang, S.; Liao, Z.; Li, X.; Zhang, X.; Chang, J. A
33 UCN@mSiO₂@cross-linked lipid with high steric stability as a NIR remote controlled-
34 release nanocarrier for photodynamic therapy. *J. Mater. Chem. B* **2015**, *3*, 3531-3540.
35
36 (146) Zhou, A.; Wei, Y.; Wu, B.; Chen, Q.; Xing, D. Pyropheophorbide A and c(RGDyK)
37 Comodified Chitosan-Wrapped Upconversion Nanoparticle for Targeted Near-Infrared
38 Photodynamic Therapy. *Mol. Pharm.* **2012**, *9*, 1580-1589.
39
40 (147) Ai, F.; Wang, N.; Zhang, X.; Sun, T.; Zhu, Q.; Kong, W.; Wang, F.; Zhu, G. An upconversion
41 nanoplatfom with extracellular pH-driven tumor-targeting ability for improved
42 photodynamic therapy. *Nanoscale* **2018**, *10*, 4432-4441.
43
44 (148) Bogdanowich-Knipp, S. J.; Chakrabarti, S.; Siahann, T. J.; Williams, T. D.; Dillman, R. K.
45 Solution stability of linear vs. cyclic RGD peptides. *J. Peptide Res.* **1999**, *53*, 530-541.
46
47 (149) Wang, Y.; Feng, M.; Lin, B.; Peng, X.; Wang, Z.; Lv, R. MET-targeted NIR II luminescence
48 diagnosis and up-conversion guided photodynamic therapy for triple-negative breast
49 cancer based on a lanthanide nanoprobe. *Nanoscale* **2021**, *13*, 18125-18133.
50
51 (150) Li, Y.; Zhang, X.; Zhang, Y.; Zhang, Y.; He, Y.; Liu, Y.; Ju, H. Activatable Photodynamic
52 Therapy with Therapeutic Effect Prediction Based on a Self-correction Upconversion
53 Nanoprobe. *ACS Appl. Mater. Interfaces* **2020**, *12*, 19313-19323.
54
55
56
57
58
59
60